

Linear and nonlinear optical properties of one-dimensional Mott insulators consisting of Ni-halogen chain and CuO-chain compounds

M. Ono, K. Miura, A. Maeda, and H. Matsuzaki

Department of Advanced Materials Science, Graduate School of Frontier Sciences, University of Tokyo, 5-1-5 Kashiwanoha, Kashiwa, Chiba 277-8561, Japan

H. Kishida

Department of Advanced Materials Science, Graduate School of Frontier Sciences, University of Tokyo and Structural Ordering and Physical Properties Group, PRESTO, Japan Science and Technology Corporation (JST), 5-1-5 Kashiwanoha, Kashiwa, Chiba 277-8561, Japan

Y. Taguchi*

Department of Applied Physics, University of Tokyo, 7-3-1 Hongo, Bunkyo, Tokyo 113-8656, Japan

Y. Tokura

Department of Applied Physics, University of Tokyo, 7-3-1 Hongo, Bunkyo, Tokyo 113-8656, Japan and Correlated Electron Research Center (CERC), National Institute of Advanced Industrial Science and Technology (AIST), Tsukuba 305-8564, Japan

M. Yamashita

Graduate School of Science, Tokyo Metropolitan University, 1-1 Minamiohsawa, Hachioji, Tokyo 192-0397, Japan

H. Okamoto[†]

Department of Advanced Materials Science, Graduate School of Frontier Sciences, University of Tokyo, 5-1-5 Kashiwanoha, Kashiwa, Chiba 277-8561, Japan and Correlated Electron Research Center (CERC), National Institute of Advanced Industrial Science and Technology (AIST), Tsukuba 305-8564, Japan

(Received 12 November 2003; revised manuscript received 12 March 2004; published 5 August 2004)

We studied the linear and nonlinear optical responses in the one-dimensional (1D) Mott insulators of the halogen (X)-bridged nickel compounds (the Ni X -chain compounds), $[\text{Ni}(\text{chxn})_2X]Y_2$ [$X, Y = \text{Cl}; X, Y = \text{Br}; X = \text{Cl}, Y = \text{NO}_3$; (chxn)=cyclohexanediamine] and the copper oxide (CuO) chain compounds, $A_2\text{CuO}_3$ ($A = \text{Sr}$ and Ca). The excitation profiles of the photoconductivity as well as the photoluminescence efficiency measurements show that charge-transfer (CT) excited states in the Ni X -chain compounds form excitonic bound states, while the excitonic effect is relatively small in Sr_2CuO_3 and negligible in Ca_2CuO_3 . The relatively large excitonic effect in the Ni X -chain compounds is attributable to the strong 1D confinement of the electronic states. The temperature dependence of the ϵ_2 spectra reveals that the spectral widths Γ_{CT} of the CT bands are dominated mainly by the electron–lattice interaction, which is smaller in the Ni X -chain compounds than in the CuO-chain ones. The $\chi^{(3)}(-\omega; 0, 0, \omega)$ spectra of the 1D Mott insulators were obtained by the electroreflectance spectroscopy. The maximum values of $|\text{Im}\chi^{(3)}(-\omega; 0, 0, \omega)|$ in the 1D Mott insulators ($\sim 10^{-5} - 10^{-8}$ esu) were considerably larger than those in other 1D semiconductors such as 1D band insulators of silicon polymers, and 1D Peierls insulators of π -conjugated polymers and halogen-bridged Pt compounds ($\sim 10^{-8} - 10^{-10}$ esu). To elucidate the enhancement of $|\text{Im}\chi^{(3)}(-\omega; 0, 0, \omega)|$ in the 1D Mott insulators, we have compared the nature of the photoexcited states of the 1D Mott insulators with those of the 1D band and Peierls insulators. In the 1D Mott insulators, the odd and even CT excited states are nearly degenerate. This degeneracy induces the large transition dipole moment between these two states and then leads to the enhancement of $\chi^{(3)}$. Such a feature in the 1D Mott insulators is independent of the magnitude of the excitonic effect, although the excitonic effect sharpens the $\chi^{(3)}$ spectrum and enhances the maximum value of $|\chi^{(3)}|$. In the 1D band and Peierls insulators, on the other hand, the splitting between the lowest excited state with odd parity and the second-lowest one with even parity is as large as the exciton binding energy. It leads to the diminution of the transition dipole moment between these two excited states and hence of $\chi^{(3)}$. These differences of the photoexcited states between the 1D Mott insulators and others have been explained in terms of the 1D extended Peierls–Hubbard model.

DOI: 10.1103/PhysRevB.70.085101

PACS number(s): 78.67.–n, 42.65.–k

I. INTRODUCTION

Nonlinear optical materials with large third-order nonlinear susceptibilities $\chi^{(3)}$ are indispensable for realization of all-optical switching, modulating and computing devices. For the development of new materials with large $\chi^{(3)}$, one of the most important strategies is to explore quasi-one-dimensional compounds, since the quantum confinement of electron-hole motion on 1D space can enhance third-order optical nonlinearity. So far two types of 1D systems have been extensively studied, i.e., the band insulators of silicon polymers,^{1–5} and the Peierls insulators of π -conjugated polymers^{6–12} and 1D halogen-bridged platinum compounds.^{13–15} Very recently, it has been reported from the electroreflectance (ER)¹⁶ and third harmonic generation (THG) spectroscopy¹⁷ that $\chi^{(3)}$ is anomalously enhanced in the 1D Mott insulators (MIs) of the halogen (X)-bridged Ni compounds (the NiX-chain compounds) and the CuO-chain ones (Sr₂CuO₃ and Ca₂CuO₃). They are insulators because of the large electron-electron Coulomb repulsion energy U on the metal sites. More exactly, they belong to charge-transfer (CT) type insulators in which a CT transition from halogen (or oxygen) to nickel (or copper) corresponds to the gap transition. Linear and nonlinear optical response is, therefore, dominated by this CT transition in these materials.

The ER study on single crystal samples of the NiX- and CuO-chain compounds has revealed that $\chi^{(3)}(-\omega; 0, 0, \omega)$ defined via the relation, $P(\omega) = 3\epsilon_0\chi^{(3)}(-\omega; 0, 0, \omega) \times \{E(0)\}^2 E(\omega)$, reaches 10^{-8} – 10^{-5} esu.¹⁶ Here, $P(\omega)$ shows nonlinear polarization, $E(0)$ the static electric field, $E(\omega)$ the electric field of light, and ϵ_0 the permittivity of vacuum. The observed $\chi^{(3)}(-\omega; 0, 0, \omega)$ values (10^{-8} – 10^{-5} esu) are considerably larger than those of the 1D band and Peierls insulators.^{13,18–20} In addition, the THG study has been performed on the single crystalline thin films of the CuO-chain compounds.¹⁷ The results have revealed that $\chi^{(3)}(-3\omega; \omega, \omega, \omega)$ defined as $P(\omega) = 1/4\epsilon_0\chi^{(3)}(-3\omega; \omega, \omega, \omega)\{E(\omega)\}^3$, is also fairly large (10^{-10} – 10^{-9} esu).

In the previous ER study, $\chi^{(3)}(-\omega; 0, 0, \omega)$ spectra are analyzed by a three-level model composed of a ground state and a pair of odd and even excited states.¹⁶ The analysis of the results has suggested that the odd and even CT states are nearly degenerate and that the enhancement of $\chi^{(3)}$ is due to a large transition dipole moment between them. The three-level model reveals important facts, but will be too simple to describe actual photoexcited states of the 1D Mott insulators. Degeneracy of the odd and even CT states has been also suggested from the peak positions of two-photon absorption (TPA)²¹ and THG¹⁷ spectra obtained for the CuO-chain compounds. The TPA and THG spectra are, however, fairly broad, so that it is difficult to deduce the detailed energy level structures of the photoexcited states directly from the experimental data.

Theoretical studies on the linear and nonlinear optical response of the 1D Mott insulators have also been performed using the one-band²² and two-band^{21,23} extended Hubbard model. The strict calculation has demonstrated that the degeneracy of the odd and even CT states and the enhancement

of the dipole moment between them are essential features of the 1D Mott insulators. In such a calculation, however, the system size is restricted to be several sites, so that it is difficult to compare the theoretical spectra directly with the experimental ones. To make possible the direct comparison between the theory and the experiment, a more simplified model called "holon-doublon model," which takes account of only the charge degree of freedom, has been proposed.^{17,22}

Thus, the extensive studies about the optical nonlinearity in the 1D Mott insulators have been performed. However, the nature of the nonlinear optical spectra and the mechanism for the enhancement of $\chi^{(3)}$ in the 1D Mott insulators have not been fully clarified yet. For the comprehensive understanding of the linear and nonlinear optical responses of the 1D Mott insulators, the important points to be solved are as follows; (1) whether the CT excited states associated with nonlinear optical response are composed of excitonic bound states or continuum states; (2) what determines the widths of linear and nonlinear optical spectra; (3) what is the physical origin for the difference of the linear/nonlinear optical responses between the 1D Mott insulators and the 1D band or Peierls insulators.

In this paper, we will report systematic investigations of the linear and nonlinear optical response on the NiX-chain compounds [Ni(chxn)₂X]Y₂ [X, Y = Cl; X, Y = Br; X = Cl, Y = NO₃; (chxn) = cyclohexanediamine] and the CuO-chain compounds A₂CuO₃ (A = Sr and Ca). After we detail the experimental procedures in Sec. II, we review the crystal and electronic structures of the 1D Mott insulators in Sec. III. In Sec. IV, we describe the results of the linear optical spectra (the imaginary part of the dielectric constant ϵ_2), the excitation profiles of the photoconductivity, and the luminescence spectra. From the results, we will deduce the effects of excitonic Coulomb interaction and electron-lattice interaction on the linear optical spectra. After that, we will report the nonlinear optical spectra [$\chi^{(3)}(-\omega; 0, 0, \omega)$] of the 1D Mott insulators obtained by the ER measurements in Sec. V. In Sec. VI, on the basis of the obtained linear and nonlinear optical spectra, we will elucidate the essential difference of the photoexcited states between the 1D Mott insulators and the other 1D semiconductors, and clarify the key factors of physical parameters, which enhance $\chi^{(3)}$ in the 1D Mott insulators. The summary of this paper is given in Sec. III.

II. EXPERIMENTAL DETAILS

Single crystals of the three NiX-chain compounds, [Ni(chxn)₂Br]Br₂, [Ni(chxn)₂Cl]Cl₂, and [Ni(chxn)₂Cl](NO₃)₂, were grown by electrocrystallization method according to the literature.^{24–26} In the following, [Ni(chxn)₂Br]Br₂, [Ni(chxn)₂Cl]Cl₂, and [Ni(chxn)₂Cl](NO₃)₂ are shown as Ni–Br–Br, Ni–Cl–Cl, and Ni–Cl–NO₃, respectively. Single crystals of the CuO-chain compounds, Sr₂CuO₃ and Ca₂CuO₃ were grown by the traveling-solvent floating-zone (TSFZ) method and the flux method, respectively.

In the polarized reflectance measurements, we used a specially designed spectrometer with a 25-cm-grating monochromator (JASCO M25-GT) and an optical microscope.

This spectrometer has a 150-W tungsten-halogen lamp and a 250-W xenon lamp as light sources, and Si and Ge photodiodes and a photomultiplier as detectors. Suitable light sources and detectors were selected depending on the measured energy range.

For the photoconductivity (PC) measurement,²⁷ the electrodes made of carbon paste were put onto the two sides of the single crystals. Light from a 150-W xenon lamp or a 150-W tungsten-halogen lamp was monochromized through a 10-cm-grating monochromator. The light was polarized by a Glan-Taylor prism and focused on the surface of the sample. In the measurements, polarization of the incident light E was parallel (\parallel) to the chain axis b . The photocurrent modulated by chopping the incident light with frequency f (~ 200 Hz) was detected by a lock-in amplifier. The spectral intensity of the lamps were corrected using a thermopile. The thickness of the sample is much larger than the absorption depths of the incident lights. Therefore, we can consider that all the incident photons were absorbed in the samples. The excitation profiles of the photoconductivity were normalized to the incident photon number by taking account of the reflection loss of the incident light. To avoid thermal effect by light irradiations, the samples were cooled to the lowest temperatures at which the photocurrent was detectable. We set the temperatures at 150 K for Ni-Cl-NO₃ and Sr₂CuO₃ and 50 K for Ni-Cl-Cl, Ni-Br-Br, and Ca₂CuO₃. In addition, we have confirmed that the chopping frequency f of the incident light is high enough ($f \sim 200$ Hz) that the contribution of thermally excited carriers is negligible compared to the photo-generated ones. Linearity of the photocurrent against the intensity of the incident light and the applied voltage (170–1000 V/cm) was also carefully checked for each sample.

For the measurements of the luminescence spectra, we used a Raman scope (RENISHAW system 1000B) equipped with He-Ne (1.96 eV) and Ar-ion laser (2.41 eV) for excitation light sources. In the measurements, polarization of the incident light is parallel (\parallel) to the chain axis b . The obtained luminescence data were corrected for the spectral response of the detection system, which was evaluated using a standard lamp. We also compared the relative efficiency of luminescence by normalizing the integrated luminescence intensity by the incident photon number.

In the ER measurements,¹⁶ two electrodes spaced about 0.5 mm out were put onto a surface of single crystalline samples and alternating electric voltage (frequency $f = 1$ kHz). The typical amplitude of the applied voltage is 1 kV. Both the applied electric field (F) and the polarization of light were set parallel to the 1D chains. The electric-field-induced change (ΔR) of the reflectivity (R) was picked out as the $2f$ component of the reflection light with a lock-in amplifier.

In all the ER measurements, samples were immersed in liquid nitrogen and kept at 77 K. In the low-temperature measurements of reflectance, photoconductivity, and luminescence, we used a conduction-type cryostat.

III. CRYSTAL AND ELECTRONIC STRUCTURES OF THE NiX CHAIN AND CuO-CHAIN COMPOUNDS

The crystal structure of [Ni(chxn)₂Br]Br₂ is presented in Fig. 1(a).²⁴ Ni³⁺ ions and X=Br⁻ ions are arranged alter-

nately along the b axis. Purely 1D electronic state is formed by the overlap of the p_z orbitals of X and the d_{z^2} orbitals of Ni [Fig. 1(c)]. Four N atoms of amino groups in two (chxn) molecules coordinate a Ni³⁺ ion in a plane normal to the chain axis b and produce a strong ligand field. A Ni³⁺ ion is therefore in a low-spin state (d^7 : spin quantum number $S = 1/2$) and one unpaired electron exists in the d_{z^2} orbital as shown in Fig. 1(e). Because of large electron-electron Coulomb repulsion energy U of 5–7 eV (Ref. 28) on the Ni ions, the Mott-Hubbard gap is opened in the Ni 3d band. The occupied Cl 3p band or Br 4p band locates between the Ni 3d upper Hubbard (UH) band and the lower Hubbard (LH) one as schematically illustrated in Fig. 1(g). The lowest optical transition corresponds to the CT transition from the halogen p valence band to the Ni 3d UH band as shown by the arrow.

The two NiCl-chain compounds, [Ni(chxn)₂Cl]Cl₂ (Ref. 29) and [Ni(chxn)₂Cl](NO₃)₂,²⁶ have similar crystal and electronic structure as [Ni(chxn)₂Br]Br₂.²⁴ The lattice parameters of the three Ni compounds are listed in Table I. Changing halogen ions X from Br to Cl decreases the lattice constant along the chains (b axis), since the ion radius of Br is larger than that of Cl. When counter ions Y are changed from Cl to NO₃ in the NiCl-chain compounds, the lattice constants in the bc plane increases. Such changes of the lattice parameters can be explained as follows. In the NiX-chain compounds, the neighboring Ni(chxn)₂ moieties on the same chain are linked by the four NH–Y–HN intrachain hydrogen (H)-bonds. The network of the H bonds extends over the chains, forming a 2D structure parallel to the bc plane. Increase of lattice constants for the Y=NO₃ compound is attributable to the increase in the size of Y and also to the decrease in the strength of the H bonds.^{30–32} The change of the lattice constant along the chain axis b , that is, the change of the Ni-X distance ($d_{\text{Ni-X}}$) by the choice of Y is expected to modify the degree of pd hybridization t_{pd} , intersite Coulomb repulsion energy V , and/or CT energy Δ .³⁰

Figure 1(b) shows the crystal structure of the CuO-chain compound, Sr₂CuO₃,³³ which is another prototype of 1D Mott insulators. 1D CuO-chains are composed of CuO₄ quadrilateral structures with sharing corner oxygens together along the b axis, in which a Cu ion is divalent ($S=1/2$) and one unpaired electron exists in the $d_{x^2-y^2}$ orbital as shown in Figs. 1(d) and 1(f). In the CuO chain, the 1D electronic state is formed by the overlap of the p_x, p_y orbitals of O and the $d_{x^2-y^2}$ orbitals of Cu.

The CuO-chain compounds are also categorized to CT insulators and the CT transition from the O 2p valence band to the Cu 3d UH band corresponds to the optical gap. Ca₂CuO₃ is isostructural to Sr₂CuO₃.³⁴ As listed in Table I, the lattice constants of Ca₂CuO₃ are smaller than those of Sr₂CuO₃ due to the smaller ion radius of Ca²⁺ than Sr²⁺. The CuO₄ quadrilateral structure of Ca₂CuO₃ is slightly distorted: The Cu–O bond lengths $d_{\text{Cu-O}}$ parallel to the chain-axis b [$d_{\text{Cu-O}}(\parallel)$] in Ca₂CuO₃ is 1.89 Å, much smaller than that in Sr₂CuO₃ (1.96 Å), while the values of $d_{\text{Cu-O}}$ perpendicular to b [$d_{\text{Cu-O}}(\perp)$] are almost equal to each other in both compounds (1.96 Å for Ca₂CuO₃, 1.96 Å for Sr₂CuO₃).^{33,34} Such a difference of the Cu–O bond length $d_{\text{Cu-O}}(\parallel)$ will also in-

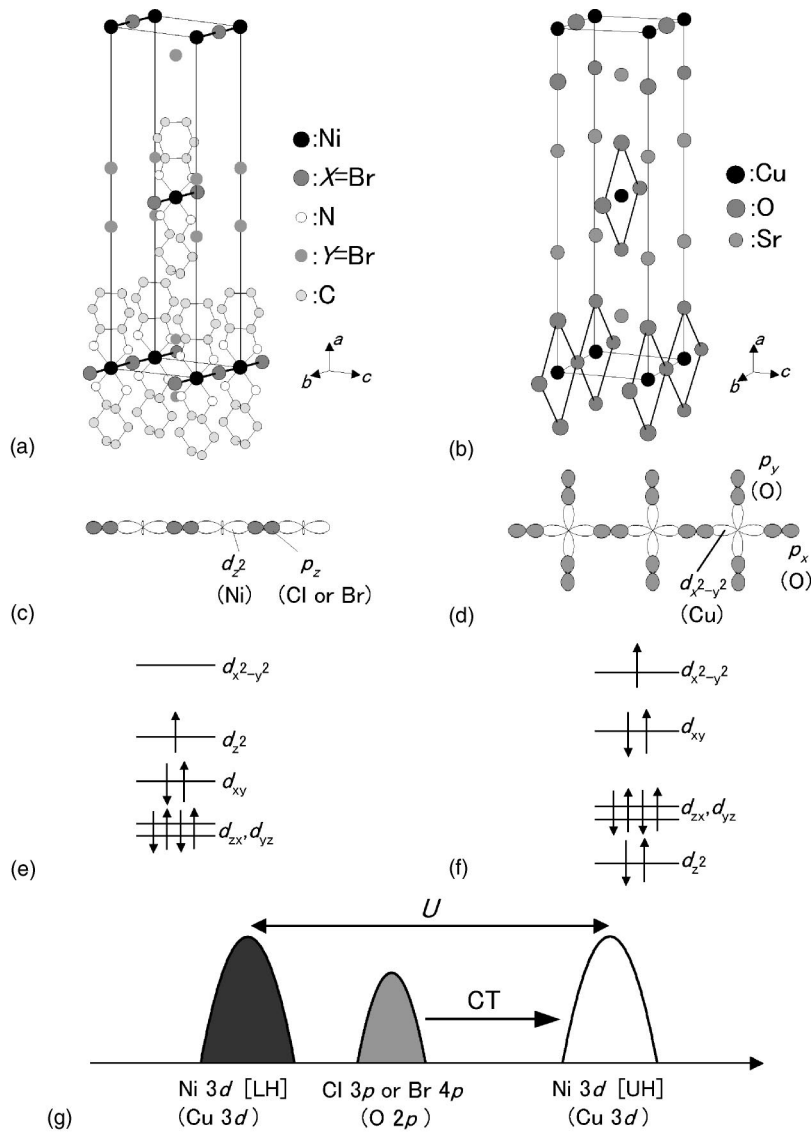


FIG. 1. Crystal and electronic structures of the halogen-bridged nickel compounds (the NiX chains) and the copper oxide chain compounds (the CuO chains). (a), (b) Crystal structure of $[\text{Ni}(\text{chxn})_2\text{Br}]\text{Br}_2$ (a) and Sr_2CuO_3 (b). (c), (d) schematic illustration of d and p orbitals forming the 1D electronic state for the NiX-chains (c) and the CuO chains (d). (e), (f), electron configuration of the d orbitals for the NiX chains (e) and the CuO chains (f). (g), schematic electronic structure of the NiX chains and the CuO chains. U is the Coulomb repulsion energy on the metal sites. CT represents the charge-transfer transition from filled p band of X(O) to empty UH d band of Ni(Cu).

duce a significant change of t_{pd} , V , and/or Δ .

Here, we will briefly mention the magnetic properties of the 1D Mott insulators. The spin susceptibility χ_{spin} in Ni-Br-Br has been previously reported from the ESR measurements.^{30,35} According to them, χ_{spin} is only slightly dependent on temperature. Its temperature dependence can be reproduced by the sum of the Bonner-Fisher curve, applicable to a 1D antiferromagnetic spin ($S=1/2$) chain, and a

contribution of small Curie component. The evaluated exchange interaction J is as large as 3600 K (Ref. 30) and 2700 K.³⁵ Our recent ESR and SQUID measurements on the Ni compounds suggest that $J=2800$ K in Ni-Br-Br, $J=2200$ K in Ni-Cl-Cl and $J=2100$ K in Ni-Cl-NO₃.³⁶ In the CuO-chains, the temperature dependence of χ_{spin} has been reported on Sr_2CuO_3 . The value of J is evaluated to be 2200 K.³⁷ Such large J values of the 1D Mott insulators

TABLE I. The lattice parameters of the NiX chain and CuO-chain compounds, $[\text{Ni}(\text{chxn})_2\text{Cl}](\text{NO}_3)_2[\text{Ni}-\text{Cl}-(\text{NO}_3)_2]$ (Ref. 29), $[\text{Ni}(\text{chxn})_2\text{Cl}]\text{Cl}_2(\text{Ni}-\text{Cl}-\text{Cl})$ (Ref. 25), $[\text{Ni}(\text{chxn})_2\text{Br}]\text{Br}_2(\text{Ni}-\text{Br}-\text{Br})$ (Ref. 24), Sr_2CuO_3 (Ref. 33), and Ca_2CuO_3 (Ref. 34). The 1D chain is along the b axis. J values of the NiX chains (Ref. 36) and Sr_2CuO_3 (Ref. 37) are evaluated from the temperature dependence of the magnetic susceptibility.

	Ni-Cl-NO ₃	Ni-Cl-Cl	Ni-Br-Br	Sr ₂ CuO ₃	Ca ₂ CuO ₃
a (Å)	22.990	23.975	23.587	12.68	12.23
b (Å) (chain)	4.982	4.894	5.161	3.91	3.77
c (Å)	8.001	6.913	7.121	3.48	3.25
J (K)	2100±500	2200±500	2800±300	2200±200	—

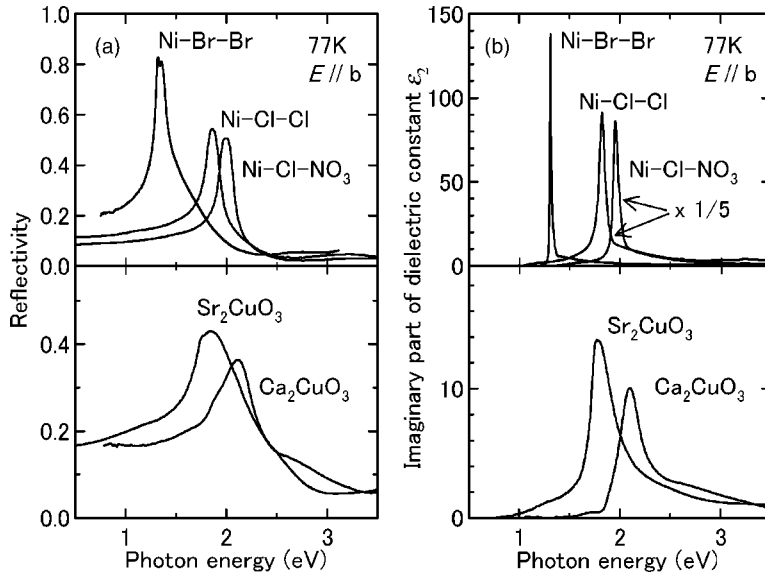


FIG. 2. (a) Polarized R spectra of three NiX-chains (Ni-Br-Br, Ni-Cl-Cl and Ni-Cl-NO₃) and two CuO chains (Sr₂CuO₃ and Ca₂CuO₃) at 77 K. The electric field (E) of lights is parallel (\parallel) to the chain axis b . (b) imaginary part of dielectric constant ϵ_2 obtained from the polarized R spectra shown in (a) by using the Kramers-Kronig transformation.

suggest the large pd hybridization along the 1D chain. Difference in the J values among the 1D Mott insulators will be discussed in Sec. IV.

IV. LINEAR OPTICAL RESPONSE IN THE NiX CHAIN AND CuO-CHAIN COMPOUNDS

A. Material dependence of CT gap energy

The polarized R spectra along the 1D chain at 77 K are presented for the five 1D Mott insulators in Fig. 2(a). Figure 2(b) shows the spectra of the imaginary part of the dielectric constant (ϵ_2), which were obtained from the R spectra by using the Kramers-Kronig (KK) transformation. Sharp peaks observed at around 1–2 eV in the ϵ_2 spectra are due to the CT transition from X to Ni (Ref. 28) or from O to Cu.³⁸ The peak energy (E_{CT}) and the spectral width (Γ_{CT}) are strongly dependent on materials. In this subsection, we will detail the dependence of E_{CT} on the three NiX-chain compounds and two CuO chains.

First, let us discuss the material dependence of E_{CT} among the three NiX-chain compounds. E_{CT} is mainly determined by Δ and t_{pd} . The obtained values of E_{CT} in the compound with $X=Br$ is by 0.5–0.6 eV smaller than that in the compounds with $X=Cl$. This is primarily due to the difference in Δ , which comes from the energy difference between the Cl 3 p orbital and the Br 4 p orbital. By changing Y from Cl to NO₃ in the NiCl-chain compounds, E_{CT} increases by about 0.15 eV. This is attributable to the increase of d_{Ni-Cl} , as mentioned in Sec. III (see Table I). As the Ni- X distance increases, Δ will decrease owing to the decrease of the Madelung site potential, which results in the decrease of E_{CT} . On the other hand, the decrease of t_{pd} with increase of d_{Ni-X} will lead to the decrease of p and d bandwidths, which gives rise to the increase of E_{CT} . The observed blueshift of the CT bands by changing Y from Cl to NO₃ as observed in Fig. 2(b) demonstrates that the latter effect, i.e., the change of t_{pd} dominates the dependence of E_{CT} on d_{Ni-X} .

The values of the exchange interaction J also give information about physical parameters. When we assume the re-

lation $U > \Delta \gg t_{pd}$, J is proportional to $t_{pd}^4 / (\Delta + V_0)^2 [1/U + 2/(2\Delta + U_p)]$,³⁹ where U_p and V_0 stand for the on-site Coulomb repulsion on the X or O site, and Coulomb repulsion between Ni site and X one or between Cu site and O one. This expression of J can be a crude measure for the degree of effective pd hybridization approximated by t_{pd}^2 / Δ , although such a perturbation treatment is insufficient for quantitative evaluation of the physical parameters. Large J (~ 2800 K) of Ni-Br-Br as compared with that of Ni-Cl-Cl and Ni-Cl-NO₃ is attributable to the smaller value of Δ . The difference of J between Ni-Cl-Cl ($J \sim 2200$ K) and Ni-Cl-NO₃ ($J \sim 2100$ K) can be explained by the increase of t_{pd} in the former compound. Thus, the observed material dependencies of J and E_{CT} are consistent with each other.

In the two CuO-chain compounds, E_{CT} of Ca₂CuO₃ is larger than that of Sr₂CuO₃. In Ca₂CuO₃, $d_{Cu-O(\parallel)}$ is smaller and the Madelung site potential is larger as compared with Sr₂CuO₃. It leads to the larger Δ in Ca₂CuO₃ than in Sr₂CuO₃. In the 2D cuprates, systematic studies have clarified that E_{CT} (or Δ) increases with decrease of Cu-O bond length.⁴⁰ The effect of the increase in t_{pd} (or bandwidth) on E_{CT} will be discussed in Sec. VI B.

B. Excitation profiles of photoconductivity

In the 1D electronic systems, the excitonic effect is sometimes anomalously enhanced.^{41–43} For example, in a band insulator of polysilane^{2–5,44} and a Peierls insulator of polydiacetylene (PDA),^{6,10,45–48,64} the binding energy of the lowest energy exciton is evaluated as ~ 1 and ~ 0.5 eV, respectively. To understand the linear and nonlinear optical responses in the 1D Mott insulators of the NiX chain and CuO-chain compounds, the information about excitonic effect is essentially important.

To evaluate the magnitude of the excitonic effect, a measurement of photoconductivity excitation spectrum is one of the most useful methods.^{49,50} In Fig. 3, the excitation profiles of photoconductivity along the chains with light polarized parallel to the chains are presented by the open circles. The

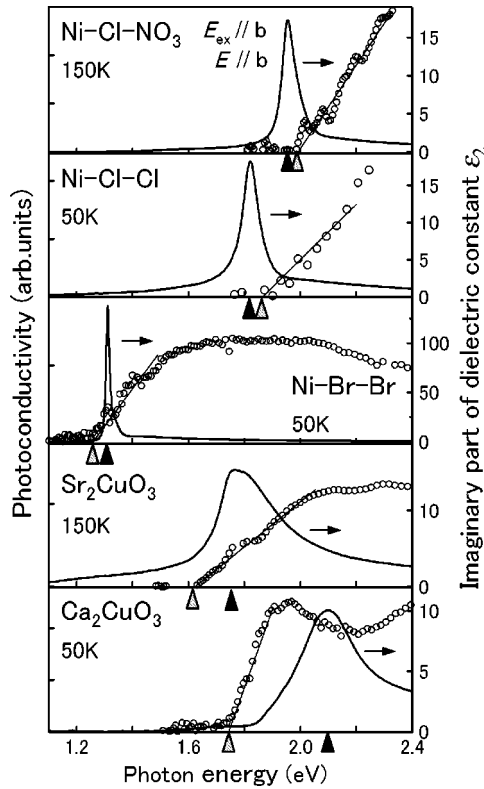


FIG. 3. Excitation profiles of photoconductivity along the chain axis b with the electric field of the excitation light $E_{ex} \parallel b$ (the open circles). Solid curves are ϵ_2 spectra for $E \parallel b$. Photoconductivity (ϵ_2) are measured at 150 K (160 K) for Ni-Cl-NO₃ and Sr₂CuO₃, and at 50 K (77 K) for Ni-Cl-Cl, Ni-Br-Br and Ca₂CuO₃. The rise of the excitation profile of photoconductivity around the band-edge is fitted by the straight lines and the threshold of photoconductivity is indicated by the grey triangles. The peak energy of the ϵ_2 spectra is denoted by the solid triangles.

photoconductivity signal with light polarized perpendicular to the chain is found to be negligibly small in both the NiX chain and CuO-chain compounds, reflecting the purely 1D nature of the electronic states. The threshold photon energy E_{th} at which the photocurrent starts to increase is indicated by the grey triangles in Fig. 3. To compare E_{th} with the peak energy of the CT band (E_{CT}), we also plotted the ϵ_2 spectra measured at the temperatures equal or close to the measurement temperatures of the respective photoconductivity spectra in Fig. 3.

In Ni-Cl-NO₃ and Ni-Cl-Cl, E_{th} is located at about 2.0 and 1.86 eV, which are larger than E_{CT} of 1.95 and 1.80 eV (indicated by the filled triangles), respectively. Excitation of the CT transition peak at E_{CT} is not sufficient for photocarrier generations. This suggests that the observed CT excited state is an excitonic bound state. On the other hand, in Ni-Br-Br, E_{th} (~ 1.25 eV) is slightly smaller than E_{CT} (~ 1.3 eV). In this compound, the absorption edge evaluated from the polarized absorption measurement is located at about 0.8 eV. In the region from 0.9 to 1.3 eV, the efficiency of the photoconductivity is very low, although most of the excitation photons are absorbed in the sample. Moreover, the photoconductivity at E_{CT} is less than 20% of the saturation

value above 1.7 eV. These results indicate that there is a finite excitonic effect in Ni-Br-Br, although it is smaller than that in the two NiCl-chain compounds.

The reason for the difference of the excitonic effects between the two NiCl-chain compounds and the NiBr chain one can be qualitatively explained as follows. Since Δ (J) in the NiCl chains are larger (smaller) than that in the NiBr chain, the effective pd hybridization, in other words, the p and d bandwidths are smaller in the NiCl chains than in the NiBr chain. Such a decrease of the bandwidth would suppress the delocalization of the photoexcited states and lead to the enhancement of the excitonic effect in the NiCl-chain compounds.

In Sr₂CuO₃, E_{th} is smaller by about 0.15 eV than E_{CT} . The photoconductivity at E_{CT} is about half of the saturation value above 2.1 eV. Therefore, the excitonic effect of Sr₂CuO₃ seems to be weaker, though not negligible, than that of Ni-Br-Br. In Ca₂CuO₃, the excitation profile of photoconductivity is considerably different from those of the other 1D Mott insulators. The photoconductivity sharply increases from the absorption edge at 1.75 eV ($=E_{th}$) and saturates at about 1.95 eV below E_{CT} . These results strongly suggest that excitonic effect is almost negligible in Ca₂CuO₃. Prominent difference of the excitonic effect between Ca₂CuO₃ and Sr₂CuO₃ is attributable to the larger t_{pd} along the 1D chain in Ca₂CuO₃, which results in the delocalization of the photoexcited states.

The results clearly show that the excitonic effect in the NiX-chain compounds is relatively larger than that in the CuO chains. Ni-Cl-Cl and Sr₂CuO₃ have the same E_{CT} and J values, so that their effective pd hybridization should be almost the same. However, the excitonic effect is much larger in Ni-Cl-Cl than in Sr₂CuO₃. Such a difference can be attributed to the difference in the chain structures. In the NiX-chains, the electronic state is composed of the d_{z^2} orbitals of Ni and the p_z orbitals of X, so that the electronic state is strongly confined in 1D space. The Coulomb interaction between photoexcited electron and hole is purely one-dimensional in character, resulting in the strong excitonic effect. In the CuO-chain compounds, 1D confinement of the electronic states is relatively weak due to the quadrilateral configuration of oxygen atoms (i.e., the $d_{x^2-y^2}$ orbital character in the UH band). Therefore, the Coulomb interaction between an electron and a hole will be less one dimensional and the excitonic effect will decrease as compared with the NiX chains.

C. Temperature dependence of ϵ_2 spectra

In this subsection, we will discuss the shapes of ϵ_2 spectra polarized along the 1D chains and their temperature dependence. First, we will compare the spectral widths Γ_{CT} of the CT band [the full width at half maximum (FWHM)] in the ϵ_2 spectra at 77 K. As shown in Fig. 2, Γ_{CT} increases in order of Ni-Br-Br, Ni-Cl-NO₃, Ni-Cl-Cl, Sr₂CuO₃, and Ca₂CuO₃. (The difference between Ni-Cl-Cl and Ni-Cl-NO₃ is small only by 0.005 eV.) In 1D electronic systems, excitonic effect concentrates a large magnitude of oscillator strength on the lowest excitonic state, resulting in a

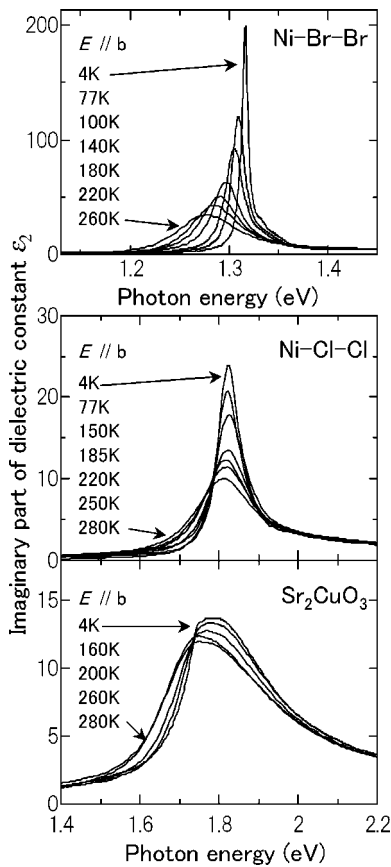


FIG. 4. Temperature dependence of the ϵ_2 spectra in Ni-Br-Br, Ni-Cl-Cl, and Sr_2CuO_3 for $E \parallel b$.

sharp absorption spectrum, as demonstrated by experimental and theoretical studies on 1D band insulators^{4,43} and 1D Peierls insulators.^{48,64,52} In the four compounds, Ni-Cl- NO_3 , Ni-Cl-Cl, Sr_2CuO_3 , and Ca_2CuO_3 , the increase of Γ_{CT} in this order seems to reflect the decrease of the excitonic effect. Among the NiX-chain compounds, Γ_{CT} in Ni-Cl-Cl or Ni-Cl- NO_3 is larger than in Ni-Br-Br, although the magnitude of the excitonic effect is relatively larger in the two NiCl-chain compounds. Therefore, the excitonic effect alone cannot fully explain the material dependence of Γ_{CT} .

To clarify the origin of the spectral width, we measured the polarized R spectra at various temperatures and obtained temperature dependence of ϵ_2 spectra. The results of Ni-Cl-Cl, Ni-Br-Br, and Sr_2CuO_3 are presented in Fig. 4. In Figs. 5(a)–5(c), we plotted Γ_{CT} by the filled circles as a function of temperature. In common to the three compounds, Γ_{CT} is independent of temperature at low temperatures and then gradually increases with temperature.

In the previous subsection, we have shown that there is a finite excitonic effect in these three materials. It is, therefore, natural that the width of the ϵ_2 spectrum and its temperature dependence is characteristic to excitonic bound states. There are three possible factors that affect the temperature-dependence of the spectral width; acoustic phonons, optical phonons, and magnons. The broadening due to acoustic phonons is generally proportional to temperature T . The existence of the plateau at low temperatures in the temperature

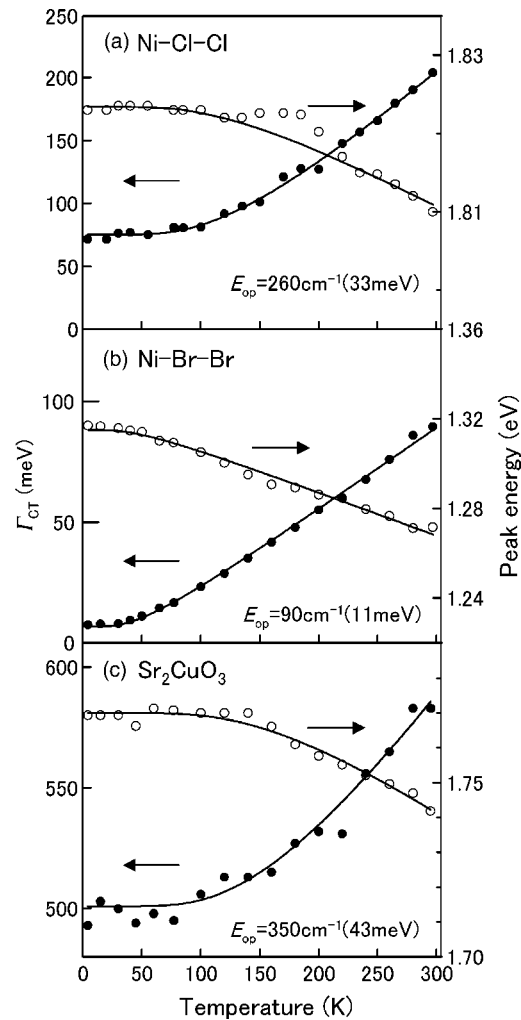


FIG. 5. Temperature dependence of the full width at half maximum (FWHM) Γ_{CT} for the ϵ_2 spectra of the CT band (the solid circles) and the peak energy of the CT band E_{CT} (the open circles) for Ni-Cl-Cl, Ni-Br-Br, and Sr_2CuO_3 . The solid lines are temperature dependence of Γ_{CT} and E_{CT} calculated by assuming the coupling of the optical phonon with photoexcited states. The energy of the optical phonon E_{OP} obtained by the fitting procedure is presented in each panel.

dependence of Γ_{CT} suggests that Γ_{CT} does not include the T -linear component as a main contribution. In the 1D Mott insulators studied here, there are spin degrees of freedom and the spin excitation has Cloizeau-Pearson-type dispersion with the energy scale of J . Contribution of exciton-magnon interaction to the spectral width will be scaled by the magnitude of J . As mentioned in Sec. III, the value of J is ~ 2800 K in Ni-Br-Br, and ~ 2200 K in Ni-Cl-Cl and Sr_2CuO_3 . When we compare Γ_{CT} between Ni-Br-Br and Ni-Cl-Cl, Γ_{CT} in Ni-Br-Br is much smaller than that in Ni-Cl-Cl. Therefore, the contribution of the exciton-magnon interaction to Γ_{CT} should not be dominant. The most plausible origin for the broadening of the spectra is the exciton-optical phonon interaction. Its contribution to the spectral width can be generalized as the following formula⁵³ including the Bose-Einstein occupation function, $n(E_{\text{OP}}/k_B T) = [\exp(E_{\text{OP}}/k_B T) - 1]^{-1}$:

TABLE II. Parameters evaluated from the analysis of the temperature dependence of ϵ_2 spectra for Ni–Cl–Cl, Ni–Br–Br, and Sr₂CuO₃. Definitions of the parameters are described in the text.

	Ni–Cl–Cl	Ni–Br–Br	Sr ₂ CuO ₃
E_{OP} (meV)	33	11	43
E_{CT}^0 (eV)	1.82	1.31	1.77
E_{CT}^1 (meV)	32.4	25.5	125
Γ_0 (meV)	75	6.9	500
Γ_1 (meV)	330	45	380

$$\Gamma_{CT}(T) = \Gamma_0 + \Gamma_1 \times n(E_{OP}/k_B T), \quad (1)$$

where Γ_0 and Γ_1 represent the contributions of temperature independent and dependent part of the broadening attributed to exciton-optical phonon interaction, respectively. E_{OP} is the energy of the optical phonon. By using this formula, we can reproduce the obtained temperature dependence of Γ_{CT} as shown by the solid lines in Fig. 5. The obtained parameters are presented in Table II.

As seen in Fig. 4, the ϵ_2 spectra of Ni–Br–Br show the low-energy shifts as well as the broadening with increase of temperature. In Ni–Cl–Cl and Sr₂CuO₃, the similar low-energy shifts are also observed. In Figs. 5(a)–5(c), temperature dependence of E_{CT} is also plotted by the open circles for the three compounds. Assuming the exciton-optical phonon interaction discussed above, the temperature dependence of the exciton peak energy E_{CT} is expressed in the generalized form as follows.⁵³

$$E_{CT}(T) = E_{CT}^0 - E_{CT}^1 \times n(E_{OP}/k_B T). \quad (2)$$

This formula also reproduces the temperature dependence of E_{CT} with the parameter values listed in Table II, as shown by the solid lines in Figs. 5(a)–5(c). The temperature dependencies of both Γ_{CT} and E_{CT} are well explained with the same values of E_{OP} . We can therefore conclude that the spectral widths of the CT bands in these compounds are dominated by optical phonons.

In the NiX–chain compounds, it is most likely that the CT exciton interacts with the longitudinal optical (LO) phonon of Ni–X stretching mode along the 1D chains. The frequency of this mode has not been known due to absence of the far-infrared (FIR) measurements and inelastic neutron scattering measurements. (No information can be obtained from Raman measurements, since the symmetric Ni–X mode is Raman inactive.) In the following, we refer to the results of the halogen-bridged Pt compounds (the PtX–chain compounds).

The PtX–chain compounds have the crystal structure similar to the NiX–chain compounds. In the PtX–chain compounds, however, the halogen ions deviate from the midpoint between two neighboring Pt ions, and the Pt²⁺ and Pt⁴⁺ arrange alternately forming a commensurate charge-density-wave (CDW) state.⁵⁴ This originates from the strong site-diagonal-type electron–lattice (e – l) interaction working between Pt and X. The lowest optical excitation of the PtX–chain compounds is the transition from Pt²⁺ to Pt⁴⁺,

which corresponds to the Peierls gap. The optical properties of the PtX–chain compounds will be discussed in detail in Secs. V and VI to compare the optical response of the 1D Peierls insulator with that of the 1D Mott insulators. The frequency of the Pt–X mode interacting with excitons has been evaluated from the time-resolved luminescence studies to be 260 cm^{−1} for the PtCl chain and 118 cm^{−1} for the PtBr chain.⁵⁵ These frequencies are very close to the E_{OP} for the Ni–Cl–Cl (260 cm^{−1}) and Ni–Br–Br (90 cm^{−1}) evaluated in this study. This fact supports the contribution of the NiX stretching LO phonon mode to the spectral broadenings and shifts of the CT bands.

In Sr₂CuO₃, E_{OP} is evaluated to be 350 cm^{−1}. In the 1D cuprates, phonon modes associated with the O atoms has been previously studied in the FIR reflectivity,⁵⁶ and Raman scattering measurements.⁵⁷ From the analysis of the FIR reflectivity spectra on Sr₂CuO₃, the frequency of the LO (TO: transverse optical) phonon has been evaluated to be 232 (181) cm^{−1}, 452 (343) cm^{−1}, 591 (550) cm^{−1}, and 577 (569) cm^{−1} (Ref. 56). The value of E_{OP} (\sim 350 cm^{−1}) is close to the frequency of the second mode, which is attributed to the bending mode associated with the Cu atoms and the O atoms locating between the Cu and Sr atoms. This bending mode might play a dominant role on the temperature dependence of Γ_{CT} and E_{CT} .

In the cuprates, the breathing-type Cu–O stretching mode is also expected to couple strongly with the CT excited states similarly to the case of the NiX–chains. Inelastic neutron scattering measurements of the 2D cuprate, La_{1.85}Sr_{0.15}CuO₄, have shown that charge excitations are strongly coupled with the zone boundary phonon of the half-breathing type Cu–O stretching mode whose activation energy is evaluated to be about 560 cm^{−1} (Ref. 58). In Ca_{1.8}Sr_{0.15}CuO₃, whose crystal structure is the same as Sr₂CuO₃, it has been pointed out from the Raman studies that the frequency of the breathing-type Cu–O stretching mode is 690 cm^{−1} (Ref. 59). This mode is located at the zone boundary and essentially Raman forbidden, but is considered to be activated near the resonance with the CT transitions. Since the frequency of the Cu–O stretching mode is much higher than room temperature (RT), it does not affect the temperature dependence of Γ_{CT} below RT. Contribution of such a high-frequency mode can be ascertained by comparing the value of Γ_0/Γ_1 . Γ_0/Γ_1 of Sr₂CuO₃ (1.33) is much larger than those of Ni–Cl–Cl (0.23) and Ni–Br–Br (0.15). The relatively large Γ_0/Γ_1 in Sr₂CuO₃ is attributable to the coupling of the high-frequency mode such as the breathing-type Cu–O stretching mode to the CT excited state, which enhances Γ_0 through spontaneous emission processes of phonons. The absolute values of Γ_0 in Sr₂CuO₃ (500 meV) is much larger than that in Ni–Cl–Cl (75 meV) and Ni–Br–Br (6.9 meV), indicating that the e – l interaction is more significant in Sr₂CuO₃ than in the NiX chains.

In Ni–Br–Br, the very small spectral width Γ_0 (6.9 meV) demonstrates the suppression of the e – l interaction. The difference of Γ_0 between the NiBr chain and NiCl–chain compounds can be qualitatively explained by the difference in the effective pd hybridization characterized by t_{pd}^2/Δ . The larger t_{pd}^2/Δ will suppress the effect of the e – l interaction in Ni–Br–Br as compared with Ni–Cl–Cl.⁶⁰

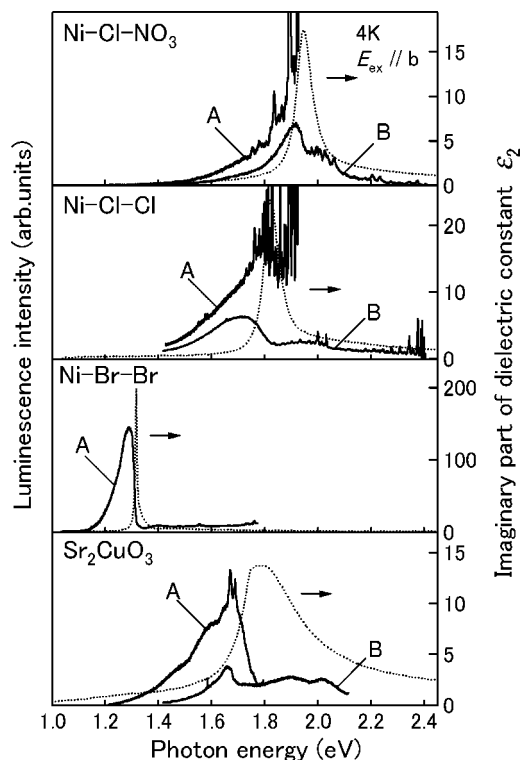


FIG. 6. Photoluminescence spectra of Ni-Cl-NO₃, Ni-Cl-Cl, Ni-Br-Br, and Sr₂CuO₃ (the solid lines) at 4 K. The spectra A and B are obtained by the excitations ($E_{ex} \parallel b$) of 1.96 and 2.41 eV, respectively. The dotted lines are the ϵ_2 spectra at 4 K.

D. Luminescence spectra

Luminescence spectroscopy is also a good probe to investigate both excitonic effect and e - l interaction. Luminescence spectra at 10 K of the four compounds, Ni-Cl-NO₃, Ni-Cl-Cl, Ni-Br-Br, and Sr₂CuO₃, are presented in Fig. 6 together with the ϵ_2 spectra at the same temperature. Luminescence of Ca₂CuO₃ is too weak to measure the spectrum. Luminescence signal is highly polarized to the chain direction. In the two NiCl-chain compounds, the luminescence spectra show excitation energy dependence. For the excitation of 1.96 eV near the CT transition peak (spectrum labeled as A), we can clearly see many sharp Raman lines overlapping on the luminescence band, which are enhanced by a resonant effect. The Stokes shift E_s of the luminescence band is very small, which is less than 0.05 eV in the two NiCl chains in common. For the excitation of 2.41 eV, the luminescence spectrum (labeled as B) shows a dip around the CT absorption peak. This dip structure is attributable to the reabsorption of the luminescence, since the absorption depth at 2.41 eV (~ 1000 Å) is considerably larger than that at the CT peak energy (~ 180 Å). In this case, the maximum of the luminescence spectrum does not necessarily give the exact peak energy of the luminescence. The real value of E_s will be smaller than the low-energy shift of the observed luminescence peak from the CT absorption peak.

In the NiBr-chain compound, the spectral shape of the luminescence will be also affected by the reabsorption effect, since the excitation energy (1.96 eV) is considerably larger

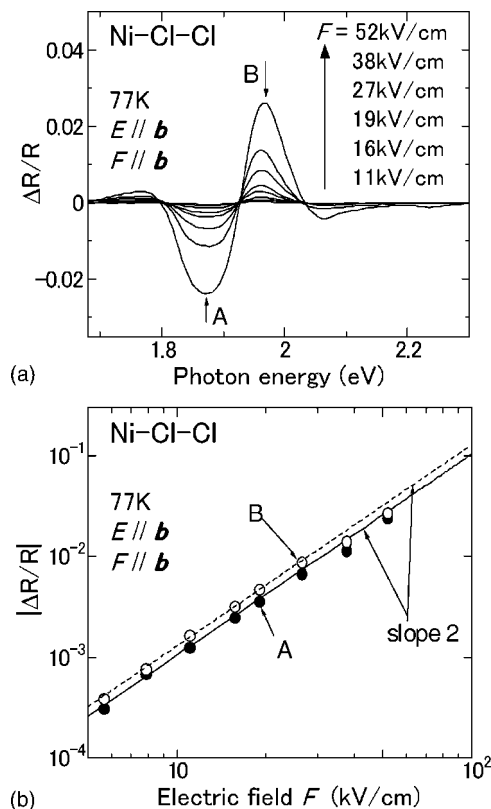


FIG. 7. (a) ER spectra $\Delta R/R$ in Ni-Cl-Cl at 77 K. Both the electric fields of light (E) and the applied electric fields (F) are parallel to b , (b) the applied-electric-field dependence of the ER signals. The solid and open circles show the $\Delta R/R$ values at two energy positions A (1.88 eV) and B (1.96 eV), respectively. The energy positions A and B are indicated by the arrows in (a). Solid and dotted lines with the slope 2 show the quadratic field dependence of the signals.

than the peak energy of CT transition. Therefore, E_s will be smaller than the observed low-energy shift of the luminescence (≈ 0.05 eV) in the NiBr-chain. Judging from these results, we conclude that the small Stokes shift E_s , which is less than 0.05 eV, is a common feature in the NiX-chain compounds.

In Sr₂CuO₃, the luminescence spectrum for the excitation of 2.41 eV is also affected by the reabsorption. For the 1.96 eV-excitation near the absorption peak, a finite Stokes shift of about 0.1 eV is clearly observed, that is in contrast with the case of the NiCl-chain compounds. This result suggests that the e - l (or exciton-phonon) interaction would play an important role in Sr₂CuO₃, as compared with the NiX-chain compounds, being consistent with the results of the temperature dependence of ϵ_2 spectra discussed in the preceding subsection.

From the integrated intensity of the luminescence and the absorption photon number of the excitation light, we have also evaluated the relative efficiency ϕ of the luminescence to be $\phi(\text{Ni-Cl-NO}_3) : \phi(\text{Ni-Cl-Cl}) : \phi(\text{Ni-Br-Br}) : \phi(\text{Sr}_2\text{CuO}_3) = 60 : 30 : 20 : 1$. This result is consistent with the tendency in the magnitude of the excitonic effect for the four compounds deduced from the excitation profiles of the photoconductivity.

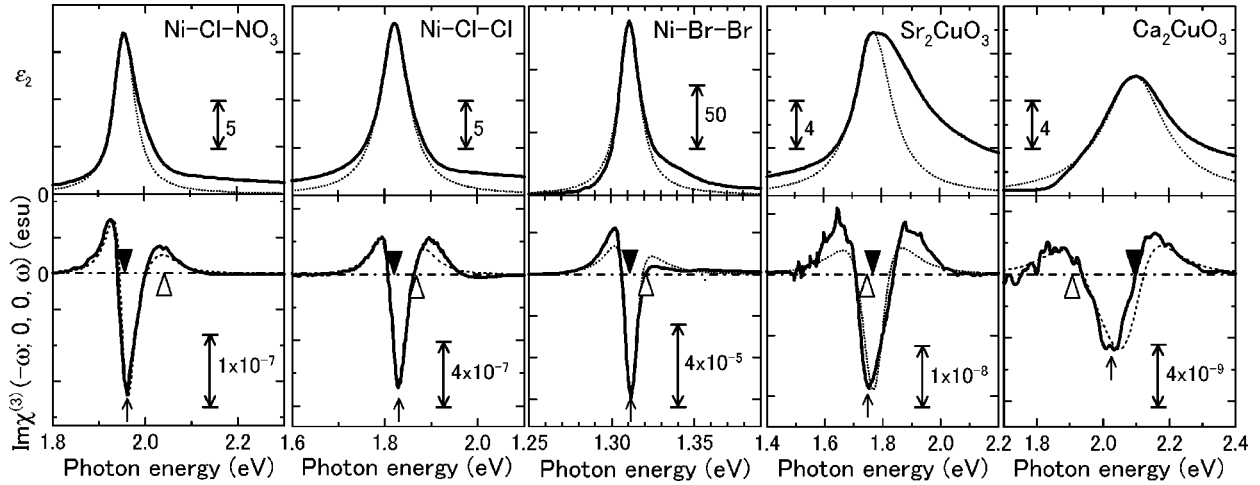


FIG. 8. $\text{Im}\chi^{(3)}(-\omega; 0, 0, \omega)$ spectra (the lower panel, the solid line) and ϵ_2 spectra (the upper panel, the solid line) at 77 K in Ni-Cl-NO₃, Ni-Cl-Cl, Ni-Br-Br, Sr₂CuO₃, and Ca₂CuO₃. The $\text{Im}\chi^{(3)}(-\omega; 0, 0, \omega)$ spectra are obtained from the $\Delta R/R$ spectra for $E\parallel b$ and $F\parallel b$ by using the KK transformation. The dotted lines in the upper panel and the lower panel show the fitting curves by the Lorentzian-type dielectric function and by the three-level model, respectively. The solid and open triangles denote the energy positions of the one-photon allowed state with odd parity and the one-photon forbidden state with even parity, respectively, which were determined by the fitting procedures. The arrows on the lower panels indicate the energy of the minimum, E_{dip} , in the $\text{Im}\chi^{(3)}(-\omega; 0, 0, \omega)$ spectra.

V. NONLINEAR OPTICAL RESPONSE IN THE NiX CHAIN AND CuO-CHAIN COMPOUNDS

To discuss third-order nonlinear optical response in a systematic way, it is necessary to evaluate $\chi^{(3)}$ spectra over a

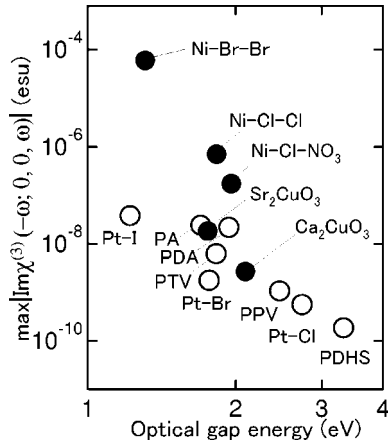


FIG. 9. Comparison of the maximum values of $|\text{Im}\chi^{(3)}(-\omega; 0, 0, \omega)|$ ($\max|\text{Im}\chi^{(3)}(-\omega; 0, 0, \omega)|$). The filled circles show the 1D Mott insulators. The open circles show other 1D semiconductors known as good third-order nonlinear optical materials, Pt-Cl: [Pt(en)₂][Pt(en)₂Cl₂](ClO₄)₄ (en=ethylenediamine) (Ref. 13), Pt-Br: [Pt(en)₂][Pt(en)₂Br₂](ClO₄)₄ (Ref. 13), Pt-I: [Pt(en)₂][Pt(en)₂I₂](ClO₄)₄ (Ref. 13), PA: polyacetylene (Ref. 18), PDA: polydiacetylene (Ref. 63), PTV: polythienylvinylene (Ref. 20), PPV: poly(*p*-phenylenevinylene), PDHS: polydihexylsilane. The data of PDHS, PA, PTV, and PPV were obtained using unoriented samples. For the other materials, single crystals of oriented films were used. To compare these values quantitatively the results for the unoriented samples with those for single crystals or oriented films, $\max|\text{Im}\chi^{(3)}(-\omega; 0, 0, \omega)|$ values of unoriented samples are multiplied by 5.

wide energy region. One of the most useful methods for this is electroabsorption (EA) or ER spectroscopy, which measures electric-field-induced change of absorption coefficient and reflectivity, respectively. This type of nonlinearity is called dc Kerr effect, which is expressed as $\text{Im}\chi^{(3)}(-\omega; 0, 0, \omega)$. In this section, we report the $\text{Im}\chi^{(3)}(-\omega; 0, 0, \omega)$ spectra of the 1D Mott insulators deduced from the ER spectroscopy.

In Fig. 7(a), we show the ER $\Delta R/R$ spectra of Ni-Cl-Cl at 77 K as a typical example. The electric-field dependencies of the signal intensity at 1.88 eV (A) and 1.96 eV (B) are presented in Fig. 7(b). The signal intensity shows a quadratic dependence on the amplitude of the applied electric field. No significant change of the spectral shape is observed by the increment of the applied electric field F from 6 to 50 kV/cm. Such a quadratic field dependence has also been ascertained for the other 1D Mott insulators studied here. Therefore, we can eliminate the possibility of the Franz-Keldysh effect as an origin of the ER signals, which is responsible for the ER signals observed around absorption edge for interband transition in conventional semiconductors.^{61,62}

By applying the KK transformation on the $\Delta R/R$ spectra, we obtained $\Delta\epsilon_2$ spectra, which were converted to $\text{Im}\chi^{(3)}(-\omega; 0, 0, \omega)$ spectra using the relation $\Delta\epsilon_2 = 3 \text{Im}\chi^{(3)}(-\omega; 0, 0, \omega)F^2$, where F is the applied electric field. In Fig. 8, we present $\text{Im}\chi^{(3)}(-\omega; 0, 0, \omega)$ spectra (the lower panel) together with ϵ_2 spectra (the upper panel) for the three NiX-chains compounds and the two CuO chain. Errors in the absolute values of $\text{Im}\chi^{(3)}(-\omega; 0, 0, \omega)$, which come from uncertainties in the estimation of the magnitude of the applied electric field, are evaluated to be less than 5%.

First, we will discuss the absolute values of $\text{Im}\chi^{(3)}$ ($|\text{Im}\chi^{(3)}|$). The maximum values of $|\text{Im}\chi^{(3)}|$ are 10^{-7} - 10^{-4} esu in the NiX-chain compounds and 10^{-8} esu in the CuO chains. In Fig. 9, the $\max|\text{Im}\chi^{(3)}|$ values of the 1D Mott insulators are plotted by the solid circles against the

optical gap (lowest exciton) energies. In the same figure, we also plotted by the open circles the $\max|\text{Im}\chi^{(3)}|$ values of other 1D semiconductors such as the band insulators of polysilane, and the Peierls insulators of π -conjugated polymers^{18,20,63} and the halogen-bridged Pt compounds (the PtX-chain compounds),¹³ which were also evaluated by the ER or EA spectroscopy. These materials are well known as good nonlinear optical materials. As clearly seen, the $\max|\text{Im}\chi^{(3)}|$ values of the 1D Mott insulators are anomalously large. In particular, the $\max|\text{Im}\chi^{(3)}|$ of Ni-Br-Br is at least three orders of magnitude larger than that of other 1D semiconductors. These results indicate that the 1D Mott insulators are prospective nonlinear optical materials.

In the $|\text{Im}\chi^{(3)}|$ spectra of the 1D Mott insulators, positive and negative components appear alternately with increase of energy in common. Such an oscillating structure has been observed in the $|\text{Im}\chi^{(3)}|$ spectra of other 1D semiconductors (polysilane,⁵ π -conjugated polymers^{12,19,47,51,64} and the PtX-chain compounds).¹³ In these materials, the observed oscillating structure has been successfully interpreted by assuming the two discrete energy levels of excited states, that is, the one-photon allowed exciton with odd parity, which is observed in the linear absorption or ε_2 spectrum, and the one-photon forbidden (two-photon allowed) exciton with even parity.⁶⁵ As shown in Sec. VI, an excitonic bound state dominates ε_2 spectrum at the absorption edge in the two NiCl-chain compounds. In Ni-Br-Br, the lowest excited state is also strongly influenced by the excitonic effect. Therefore, it is reasonable to analyze $|\text{Im}\chi^{(3)}|$ spectra of the three Ni compounds by using the three-level model composed of the ground state, the odd excited state, and the even excited state as shown in Fig. 10(a).

In the analysis, we performed the parameter fitting on the ε_2 spectrum by assuming the following Lorentzian-type dielectric function:⁶⁶

$$\varepsilon_{\text{CT}}(\omega) = \frac{Ne^2}{\hbar} \langle 0|x|1\rangle \langle 1|x|0\rangle \left(\frac{1}{\omega_1 - \omega - i\gamma_1} + \frac{1}{\omega_1 + \omega + i\gamma_1} \right), \quad (3)$$

where \hbar is the Planck constant and e is the electron charge. $|0\rangle$ and $|1\rangle$ show the ground state and the one-photon allowed excited state with odd parity, respectively, and $\langle 0|x|1\rangle$ shows the transition dipole moment between them. ω_1 and γ_1 are the energy and the damping factor for the state $|1\rangle$. γ_1 corresponds to half of Γ_{CT} . The calculated curves are shown by the dotted lines in the upper panel of Fig. 8, which closely reproduce the observed CT bands in the three NiX-chain compounds. The obtained parameters are summarized in Table III.

In the three-level model, $\chi^{(3)}$ is given from the perturbation theory. The main term dominating the spectral shape of $\chi^{(3)}$ is expressed as follows:⁶⁶

$$\begin{aligned} \chi^{(3)}(-\omega; 0, 0, \omega)_{\text{main}} \\ = \frac{Ne^4}{3\varepsilon_0\hbar^3} \frac{\langle 0|x|1\rangle \langle 1|x|2\rangle \langle 2|x|1\rangle \langle 1|x|0\rangle}{(\omega_1 - \omega - i\gamma_1)(\omega_2 - \omega - i\gamma_2)(\omega_1 - \omega - i\gamma_1)}, \end{aligned} \quad (4)$$

where $|2\rangle$ shows the one-photon forbidden excited state with

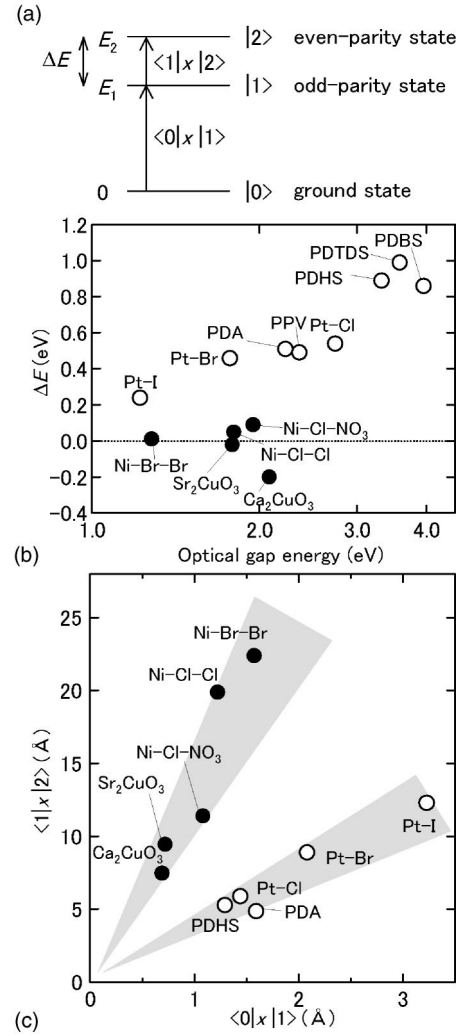


FIG. 10. (a) The schematic illustration of the three-level model used for the analysis of the $\text{Im}\chi^{(3)}(-\omega; 0, 0, \omega)$ spectra. ΔE is the energy splitting between the one-photon allowed excited state $|1\rangle$ with odd parity (E_1) and the one-photon forbidden excited state $|2\rangle$ with even parity (E_2). $\langle 0|x|1\rangle$ and $\langle 1|x|2\rangle$ are the dipole moments between the ground state $|0\rangle$ and $|1\rangle$ and between $|1\rangle$ and $|2\rangle$, respectively. (b) The energy splitting ΔE is plotted as a function of the optical gap energy for various 1D semiconductors. Abbreviations and references for Pt-I, Pt-Br, and Pt-Cl are the same as those used in Fig. 9. As for the conjugated polymers. We referred to the results of ER measurement for PDA in Ref. 19, EA measurement for polysilanes (PDHS: polydihexylsilane, PDTDS: polyditetradecylsilane, PDBS: polydibutylsilane) in Ref. 5. The datum of PPV is derived from the two-photon absorption measurement in Ref. 68. (c) The relation between the transition dipole moments, $\langle 0|x|1\rangle$ and $\langle 1|x|2\rangle$, for various 1D materials. The filled circles and the open circles show the 1D Mott insulators and other 1D semiconductors, respectively. Abbreviations and references for Pt-I, Pt-Br, Pt-Cl, and PDA are the same as those we used in Fig. 9. The datum for PDHS is obtained in this work (Ref. 69).

even parity and $\langle 1|x|2\rangle$ the dipole moment between $|1\rangle$ and $|2\rangle$. ω_2 and γ_2 are the energy and the damping factor for the state $|2\rangle$, respectively, N is the density of the metal atoms. To be more exact, $\chi^{(3)}$ is composed of 12 independent terms

TABLE III. Parameters evaluated from the analysis of the $\text{Im}\chi^{(3)}(-\omega; 0, 0, \omega)$ spectra at 77 K by the three-level model in the NiX chain and CuO-chain compounds. E_1 and E_2 are the energy of the one-photon allowed state with odd parity and the one-photon forbidden state with even parity. $\langle 0|x|1 \rangle$ and $\langle 1|x|2 \rangle$ are the transition dipole moments between the ground state and the odd excited state, and between the odd and even excited states, respectively. γ_1 and γ_2 are the damping factors for the odd and even excited states, respectively. $|\text{Re}\chi^{(3)}(-\omega; \omega, -\omega, \omega)|$ at the optical communication wavelength ($1.55 \mu\text{m}$) was calculated by using the parameters.

	Ni-Cl-NO ₃	Ni-Cl-Cl	Ni-Br-Br	Sr ₂ CuO ₃	Ca ₂ CuO ₃
E_1 (eV)	1.95	1.82	1.311	1.77	2.1
$\langle 0 x 1 \rangle$ (Å)	1.08	1.23	1.58	0.717	0.688
E_2 (eV)	2.04	1.87	1.321	1.75	1.9
$\langle 1 x 2 \rangle$ (Å)	11.4	19.9	22.4	9.45	6.8
$\Delta E = (E_2 - E_1)$ (eV)	0.09	0.05	0.010	-0.02	-0.2
γ_1 (meV)	0.027	0.036	0.0073	0.078	0.11
γ_2 (meV)	0.055	0.053	0.038	0.2	0.1
$ \text{Re}\chi^{(3)}(-\omega; \omega, -\omega, \omega) $ (esu) at $1.55 \mu\text{m}$	6.3×10^{-11}	4.9×10^{-10}	1.5×10^{-9}	1.0×10^{-10}	7.5×10^{-11}

including Eq. (4) as the major term.⁶⁶ By using the complete expression of $\chi^{(3)}$, we performed a parameter fitting of $\text{Im}\chi^{(3)}$ spectrum. For the parameters, $\langle 0|x|1 \rangle$, ω_1 and γ_1 , we used the values obtained from the fitting procedures of the ε_2 spectra.⁶⁷ The calculated $\text{Im}\chi^{(3)}$ spectra are presented by the broken lines in the lower panels of Fig. 8, which reproduce well the experimental results for the NiX-chain compounds. The obtained parameters are summarized in Table III.

From these analyses, we can find two important features of the photoexcited states in the NiX-chain compounds. The first feature is associated with the energy splitting [$\Delta E = \hbar(\omega_2 - \omega_1)$] between the odd and even excited states. In Fig. 8, the energy positions of the odd and even excited states are indicated by the solid and the open triangles, respectively. ΔE is very small, which is 90 meV in Ni-Cl-NO₃, 50 meV in Ni-Cl-Cl, and 10 meV in Ni-Br-Br. The second feature is that the dipole moments $\langle 1|x|2 \rangle$ is very large. Note that $\langle 1|x|2 \rangle / \langle 0|x|1 \rangle$ exceeds 10. ΔE as a function of the optical gap (lowest exciton) energy, and the dipole moments $\langle 0|x|1 \rangle$ and $\langle 1|x|2 \rangle$ are presented in Figs. 10(b) and 10(c).

In the 1D band insulators of polysilane, and the 1D Peierls insulators of π -conjugated polymers and the PtX-chain compounds, the energy position of the even-parity exciton has been determined from the results of TPA spectroscopy⁶⁸ as well as the ER or EA spectroscopy, by taking account of the three-level model.^{5,13,19} The energy splitting (ΔE) between the odd and even exciton states of these 1D semiconductors is plotted in Fig. 10(b). The quantitative evaluation of the transition dipole moments, $\langle 0|x|1 \rangle$ and $\langle 1|x|2 \rangle$, has been performed for polydihexylsilane (PDHS),⁶⁹ the PtX-chain compounds⁷⁰ and polydiacetylene (PDA).¹⁹ The results are also presented in Fig. 10(c), together with the results of the 1D Mott insulators.

In these 1D band and Peierls insulators, the excited states with even parity identified from the nonlinear spectroscopy have been revealed to be excitonic bound states. Therefore, ΔE gives a lower limit of the exciton binding energy E_b . Judging from the values of ΔE shown in Fig. 10(b), E_b of these materials are very large, which ranges from 0.2 to 1eV.

These values are much larger than those of the 1D Mott insulators, which are less than 0.1 eV as deduced from the results of the photoconductivity excitation spectra presented in Fig. 3. As for the dipole moments of the 1D band and Peierls insulators, $\langle 1|x|2 \rangle / \langle 0|x|1 \rangle$ is almost equal to 3 and $\langle 1|x|2 \rangle$ is not so large as compared with those of the 1D Mott insulators as seen in Fig. 10(c).

In Eq. (4) based on the three-level model, the important factors dominating $\max|\text{Im}\chi^{(3)}|$ are the transition dipole moments; $\text{Im}\chi^{(3)}$ is proportional to $(\langle 0|x|1 \rangle \langle 1|x|2 \rangle)^2$. The dipole moment $\langle 1|x|2 \rangle$ in the 1D Mott insulators are considerably larger than those in the band and Peierls insulators. It suggests that the large $\langle 1|x|2 \rangle$ is the important origin for the enhancement of $\chi^{(3)}$ in the 1D Mott insulators. The other important factors determining the values of $\max|\text{Im}\chi^{(3)}|$ are the damping factors ($\gamma_{1,2}$) and ΔE . Assuming the resonance condition ($\omega = \omega_1$), one can easily see from the denominator of Eq. (4) that the decrease of $\gamma_{1,2}$ and ΔE should enhance $\max|\text{Im}\chi^{(3)}|$. Actually, both γ_1 and ΔE in the NiX-chain compounds are relatively small as compared with those of PDHS ($\gamma_1 = 0.14$ and $\Delta E = 0.89$ eV)⁶⁹ and the PtX chains ($\gamma_1 = 0.22$ eV and $\Delta E = 0.54$ eV for $X = \text{Cl}$, $\gamma_1 = 0.23$ eV and $\Delta E = 0.46$ eV for $X = \text{Br}$, $\gamma_1 = 0.15$ eV and $\Delta E = 0.24$ eV for $X = \text{I}$),¹³ and PDA ($\gamma_1 = 0.027$ eV and $\Delta E = 0.51$ eV),¹⁹ which would also be responsible for the enhancement of $|\text{Im}\chi^{(3)}|$ in the NiX-chain compounds.

We have also performed the similar analysis for Sr₂CuO₃ and Ca₂CuO₃, in which the excitonic effect is small and negligible, respectively. As shown in the upper panel of Fig. 8, there are some discrepancies at the high-energy side of the ε_2 peaks between the experimental ε_2 spectrum (the solid line) and the calculated one (the broken line) based on Eq. (4). The calculated $\text{Im}\chi^{(3)}$ spectra shown by the broken lines in the lower panel of Fig. 8 reproduce the characteristic oscillating structure of the experimental spectra, although there are also slight deviations. The energy positions of the odd and even states are also indicated in Fig. 8 by the solid and open triangles, respectively, and the parameters are summarized in Table III. The value of $\langle 1|x|2 \rangle$ is 10 times as much as $\langle 0|x|1 \rangle$ (similar to the case of the NiX-chain compounds).

ΔE and the dipole moments, $\langle 0|x|1\rangle$ and $\langle 1|x|2\rangle$, are also plotted in Figs. 10(b) and 10(c) for the two CuO-chain compounds. The discrepancy between the experimental results and calculated ones suggests that the three-level model assuming the two excited states are not sufficient to explain the optical response. The contribution of the continuum or multielectron-excited states should be taken into account for the analysis of the $\text{Im}\chi^{(3)}$ spectra in the two CuO chains. As for this problem, we will discuss in Sec. VI B.

VI. DISCUSSIONS

A. Comparison of linear and nonlinear optical response between 1D Mott insulators and other 1D semiconductors

As reported in the previous sections, there are three important differences in the nature of photoexcited states and the nonlinear optical response between the 1D Mott insulators and other 1D semiconductors.

(1) The binding energy E_b of the excitonic bound states in the 1D Mott insulators is smaller than that in the 1D band and Peierls insulators.

(2) The splitting ΔE between the odd and even excited states is small in the 1D Mott insulators and large in the 1D band and Peierls insulators.

(3) The transition dipole moment between the odd and even excited state $\langle 1|x|2\rangle$ is large in the 1D Mott insulators but relatively small in the 1D band and Peierls insulators. The large $\langle 1|x|2\rangle$ is the most important origin for the enhancement of $\chi^{(3)}$ in the 1D Mott insulators.

In this section, we will discuss the origins of these differences.

First, we will compare qualitatively the photoexcited states of the 1D band insulators with those of the 1D Mott insulators. To discuss the optical response of the 1D band insulators, we use a simple molecular-orbital image⁷¹ illustrated in the upper part of Fig. 11(a). In this model, 1D electronic state is composed of the highest occupied molecular orbitals and the lowest unoccupied ones. The intramolecular excitation indicated by the open arrow corresponds to the lowest excited state ($|1\rangle$) with odd parity. The in-phase combination of the intermolecular CT excitations indicated by the broken arrows corresponds to the second-lowest excited state ($|2\rangle$) with even parity. Excited electron and holes occupy the same site in the lowest odd excited state, but on different sites in the second lowest even excited state. The lowest odd excited state forms an exciton with large binding energy due to the large electron-hole Coulomb attractive interaction, and then the energy splitting ΔE between the lowest odd and second-lowest even excited states is considerably enhanced. The envelopes of the exciton wave functions are schematically illustrated in the lower part of Fig. 11(a). There is a large difference of the spatial extension of the wave functions between the odd and even excited states, which is unfavorable for obtaining a large dipole moment $\langle 1|x|2\rangle$. As a result, $\chi^{(3)}$ is not so large. The detailed theoretical studies have indeed demonstrated that these features deduced from the simple physical image shown in Fig. 11(a) can explain the linear and nonlinear optical responses of polysilane.⁴

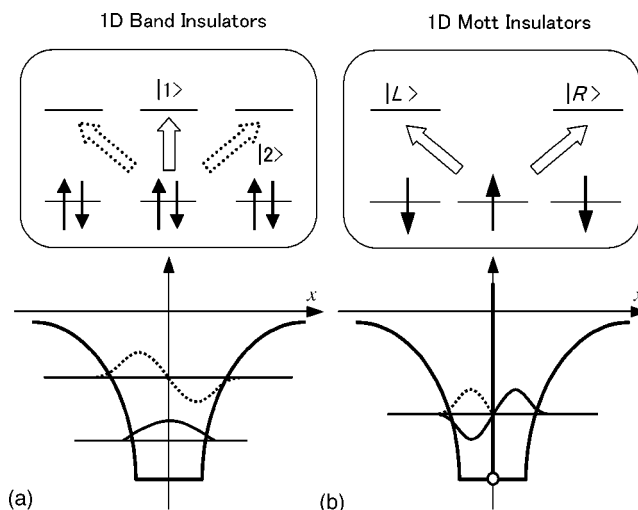


FIG. 11. (a) A simple molecular-orbital image representing the photoexcited states of a 1D band insulator. The highest occupied molecular orbital and the lowest unoccupied one are drawn by the bars in the upper panel. Electrons (spins) are shown by the up and down solid arrows. The open and dotted arrows indicate the intra- and intermolecular excited states, respectively. The intramolecular excitation is the lowest one-photon allowed transition to the intramolecular exciton state. The in-phase combination of the intermolecular excitations with the opposite directions corresponds to the second lowest exciton state, which is optically forbidden. The envelope functions of the lowest and second lowest exciton states are schematically drawn with the solid and broken lines in the lower figure, (b) a half-filled single-band Hubbard model representing the photoexcited states of a 1D Mott insulator. The intersite transitions to the right and the left are expressed as $|R\rangle$ and $|L\rangle$, respectively. The in-phase and out-of-phase combination of $|R\rangle$ and $|L\rangle$ corresponds to the even and odd excited states, respectively. The lower panel shows the wave functions for these two excited states.

To discuss the linear and nonlinear optical responses of the 1D Mott insulators, we consider a half-filled single-band Hubbard model illustrated on the upper part of Fig. 11(b). It has been well established that this model can describe the CT excitations in the CuO chains by mapping a Zhang-Rice state onto the LH band.^{39,72} For the recent angle-resolved photoemission spectra of the NiBr-chain compound, the analysis using the two-band model (or equivalently the d - p chain model) has been successfully made.⁷³ In the NiBr chain, the d - p chain model should be more effective because of the small value of Δ . However, for simplicity, we adopt the single-band Hubbard model to discuss the optical responses of the NiX chains. It will be sufficient to reveal their fundamental features. In the previous studies, the single-band Hubbard model has been applied to the NiX-chain compounds and explains the characteristic behaviors of the luminescence associated with the CT excitations.⁶⁰

In a simplified image, the odd and even excited states ($|1\rangle$ and $|2\rangle$) of these 1D Mott insulators correspond to the out-of-phase and in-phase combination of the two intersite excitations $|R\rangle$ and $|L\rangle$ with opposite directions as shown on the upper part of Fig. 11(b). In the case that U is much larger than the transfer energy t , the energy splitting ΔE between the odd and even excited states will be small and the wave

functions of the two states are very similar to each other except for their phases. The wave functions for $U \gg t$ are schematically illustrated on the lower part of Fig. 11(b).⁷⁴ In this case, there is a large spatial overlap of the wave functions between the odd and even excited states, which leads to a large dipole moment $\langle 1|x|2 \rangle$ and then to a large $\chi^{(3)}$.

The parameter values in the single-band extended Hubbard model for Sr_2CuO_3 have been evaluated to be $t = 0.55$ eV, $U = 4.2$ eV, and the intersite Coulomb repulsion energy $V = 1.3$ eV from the analysis of electron energy loss spectroscopy.⁷⁵ For the NiX-chain compounds, they have been evaluated to be $t = 0.3$ eV, $U = 2.72$ eV, and $V = 1$ eV for Ni–Br–Br from the analysis of the optical spectra and the J value.⁶⁰ These parameter sets give large U/t , which is 8–9. These large U/t values suggest that the simplified image in Fig. 11(b) would stand in the 1D Mott insulators studied here.

Next, let us compare the photoexcited states of the 1D Peierls insulators with those of the 1D Mott insulators. As for the excited states for π -conjugated polymers, a large number of theoretical studies have been reported. Abe *et al.*^{10,52} have calculated the one-electron tight-binding Hamiltonian and showed that, in the Peierls insulator, excitonic effect is fairly large in the lowest odd-parity state and is rather small in the lowest even-parity state, which leads to a large splitting ΔE between these two states. Moreover, it is shown by Shuai *et al.*⁷⁶ and Gallagher *et al.*⁷⁷ that, even with the strong electronic correlation U , ΔE , and E_b become large with the finite bond alternation. These theoretical studies explain both large E_b and large ΔE in conjugated polymers.

To see directly the difference of E_b and ΔE between 1D Peierls insulators and Mott insulators, it is appropriate to compare those parameters between the PtX-chain compound and the NiX-chain compound, since these two types of compounds have the similar chain structure.

In the NiBr-chain compound, ΔE is evaluated to be 10 meV from the analysis of the ER spectrum (see Table III). The result of the photoconductivity excitation spectrum in Fig. 3 demonstrates a very small E_b , which will be almost the same as ΔE . In the PtI-chain compound $[\text{Pt}(\text{en})_2][\text{Pt}(\text{en})_2\text{I}_2](\text{ClO}_4)_4$, on the other hand, ΔE is 0.24 eV [see Fig. 10(b)] and E_b is larger than 0.5 eV judging from the result of the photoconductivity excitation spectrum previously reported.⁷⁸ Although these two compounds have almost the same optical gap ($=1.3$ – 1.4 eV), the difference in ΔE and E_b is fairly large.

To clarify the difference between the PtX and the NiX chain, we adopt a simple model of the photoexcited states based upon the Peierls–Hubbard model. The model for the PtX chain is illustrated in Fig. 12(a). We assume that divalent metal site and quadrivalent one are arranged alternately and shown in Fig. 12(a-1). Photoexcited electron and hole, both of which form trivalent sites, occupy only the originally quadrivalent sites and divalent sites, respectively. The transfer integral of an electron (a hole) between neighboring divalent (quadrivalent) metal sites (or equivalently the next nearest neighbor sites) is defined as t_C . The Coulomb interaction ($-V$) between an electron and a hole located on the neighboring two Pt sites is taken into account. The Hamil-

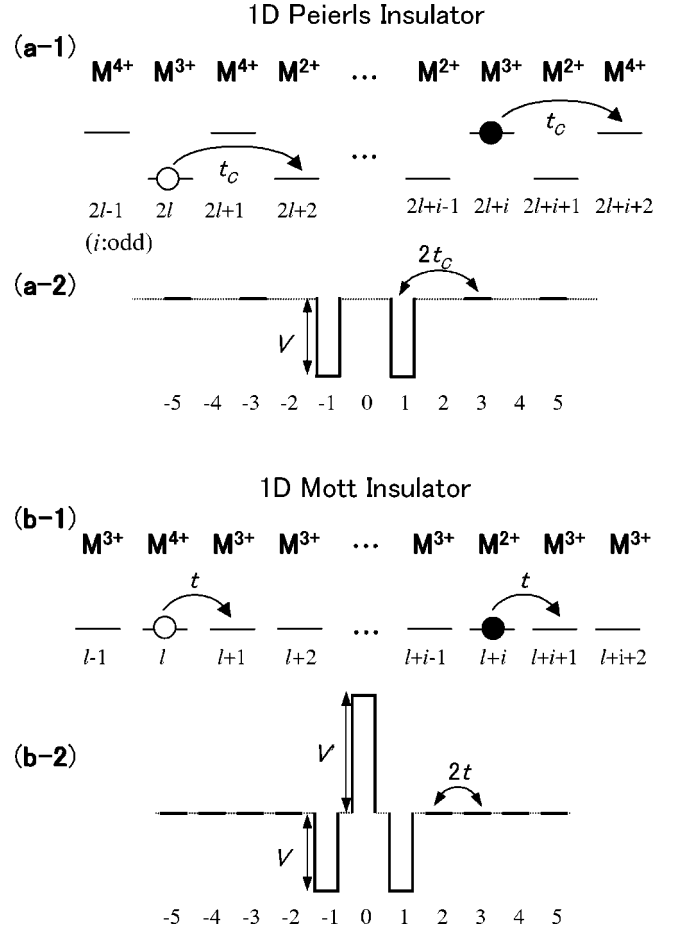


FIG. 12. (a-1) Schematic image for an excitation of an electron-hole pair in a 1D Peierls insulator. The excited electron and hole occupy the originally quadrivalent (odd-number) and divalent (even-number) sites, respectively. t_C is the transfer energy between the neighboring odd (or even) sites. (a-2) Schematic illustration of a two-impurity model describing an electron-hole pair excitation in a 1D Peierls insulator. V is the electron-hole Coulomb attractive energy. Note that only the odd-number sites are drawn, because electrons cannot hop to the even sites, (b-1) schematic image for an excitation of an electron-hole pair in a 1D Mott insulator. t is the transfer energy between the neighboring sites. An electron and a hole cannot occupy the same site. (b-2) Schematic illustration of a three-impurity model describing an electron-hole pair excitation in a 1D Mott insulator. V is the electron-hole Coulomb attractive energy. V' prohibits the occupation of an electron and a hole on the same site.

tonian for the photoexcited electrons and holes is given as follows:

$$H_{PI} = t_C \sum_{l,\sigma} (a_{2l+1,\sigma}^+ a_{2l-1,\sigma} + \text{h.c.}) + t_C \sum_{l,\sigma} (b_{2l+1,\sigma}^+ b_{2l-1,\sigma} + \text{h.c.}) - V \sum_{l,\sigma} (n_{2l+1,\sigma}^a n_{2l,-\sigma}^b + n_{2l,-\sigma}^b n_{2l+1,\sigma}^a), \quad (5)$$

where $a_{2l+1,\sigma}^+$ and $a_{2l+1,\sigma}$ are the creation and annihilation operators for an electron at the odd number ($2l+1$) sites, respectively. σ denotes the spin quantum number. σ and $-\sigma$ represent the spins with opposite directions. $b_{2l,\sigma}^+$ and $b_{2l,\sigma}$

are the creation and annihilation operators for a hole at even number ($2l$) sites with spin σ . h.c. denotes hermite conjugate. $n_{l,\sigma}^a$ and $n_{l,\sigma}^b$ are number operators of electron and hole with spin σ , respectively. Here we consider only the $\mathbf{k}=0$ subspace, where \mathbf{k} represents the center-of-mass momentum of the hole and the electron. In this case, the Hamiltonian [Eq. (5)] can be reduced to a simple two-impurity model, which is shown in Fig. 12(a-2). The details of the transformation procedures are given in the Appendix.

For the 1D Mott insulator, the presence of spin degrees of freedom makes it difficult to discuss quantitative nature of the photoexcited states. It has, however, been suggested that in the strong coupling limit ($U \gg t$), the spin degrees of freedom can be removed from the problem, because of the concept of the spin-charge separation.⁷⁹ Mizuno *et al.* have shown that an effective two-particle model with only the charge degrees of freedom is appropriate to deal with the optical responses of the 1D Mott insulators.²² That model is called the holon-doublon model,⁸⁰ since the charge degrees of freedom of excited hole (an unoccupied site) and electron (a doubly occupied site) are called holon and doublon, respectively. In this conjecture, two particles cannot occupy the same site and, therefore, the odd and even excited states are always degenerate.

On the basis of the holon-doublon model, we will discuss the excitonic properties of the 1D Mott insulators. We consider a simplified model shown in Fig. 12(b-1), keeping the NiX chain in our minds. The Hamiltonian is given by

$$H_{MI} = t \sum_l (a_{l+1}^+ a_l + \text{h.c.}) + t \sum_l (b_{l+1}^+ b_l + \text{h.c.}) - V \sum_l (n_{l+1}^a n_l^b + n_l^b n_{l-1}^a) + V' \sum_l n_l^a n_l^b, \quad (6)$$

where t and $-V$ are the transfer integral between the nearest neighbor sites and the Coulomb attractive interaction between the neighboring holon and doublon, respectively. In the last term, we set V' to be infinity. This leads to the feature that a holon and a doublon cannot occupy the same site. When we consider only the $\mathbf{k}=0$ subspace, this model boils down to a simple three-impurity model shown in Fig. 12(b-2) (see the Appendix).

The two- or three-impurity problems can be solved exactly,⁸¹ and the eigenvalues and wave functions can be analytically obtained. The calculated binding energy of the trapped state (E_b) is plotted as a function of V in Fig. 13. In this figure, we set the absolute value of t as unity and all the other parameters are normalized by t . Note that t_C (the transfer energy between the next nearest neighbor sites) in the Peierls insulator should be much smaller than t (the transfer energy between the nearest neighbor sites). When the site energy difference between the divalent and quadrivalent sites (δ) is much larger than t , t_C will be the order of t^2/δ . Here, we select $t_C=0.02$ which corresponds to $\delta \sim 5$.⁸²

As seen in Fig. 13, two degenerate bound states with odd and even parity are stabilized for $V > 2t$ in the 1D Mott insulator. There is no bound state for $V < 2t$. Such a change in the stability of the excitonic bound state has been demonstrated by more strict theoretical studies of the 1D Mott in-

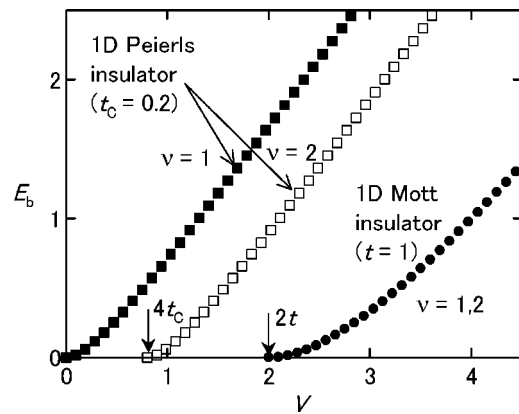


FIG. 13. Binding energies E_b of an electron-hole pair as a function of V in a 1D Peierls insulator ($t_C=0.2$) and a 1D Mott insulator ($t=1$). The solid and open squares are E_b for the lowest excited state with odd parity ($\nu=1$) and the second lowest excited state with even parity ($\nu=2$) in a 1D Peierls insulator. The solid circles denotes E_b in a 1D Mott insulator, where the odd ($\nu=1$) and even ($\nu=2$) excited states are degenerate.

ulators based upon the extended Hubbard model with large U/t .^{17,75,80,83,84} In the 1D Peierls insulator, on the other hand, the lowest excited state ($|1\rangle$) with odd parity is always a bound state for a finite V . The second-lowest excited state ($|2\rangle$) with even parity is also a bound state for $V > 4t_C$. In this case, there is a large splitting between the two bound states, that is equal to $4t_C$. The binding energy E_b of the lowest excited state is much larger in the 1D Peierls insulator than in the 1D Mott insulator.⁸⁵

The theoretical expectations presented here explain the difference of ΔE and E_b between the NiBr and PtX chains. Figure 14 shows the wave functions of the odd and even excited states in the 1D Peierls insulator and the 1D Mott insulator obtained from the simple models discussed above. The spatial extensions of the wave functions for the odd and even excited states are different from each other in the 1D Peierls insulator, with the result that the dipole moment $\langle 1|x|2\rangle$ and hence the magnitude of $\chi^{(3)}$ will be relatively small as compared with the 1D Mott insulator. The comparison of Fig. 14(a) with Fig. 11(a) clearly shows that the nature of the photoexcited states for the 1D Peierls insulator is similar to that for the 1D band insulator. This is the reason why the linear and nonlinear optical responses of the PtX-chain compounds are similar to those of polysilane.

The holon-doublon model seems to be an effective model for the photoexcited state of the 1D Mott insulators, since it can explain small binding energy of an exciton as well as degeneracy of the odd and even excited states. Strictly speaking, however, the condition of $U \gg t$ does not perfectly fit the 1D Mott insulators studied here, since t/U is finite (≥ 0.1) and J is fairly large ($\sim 2000-3000$ K). Such large values of J suggest that the model including the spin degrees of freedom should explain more precisely the linear/nonlinear optical properties of the 1D Mott insulators, although the spin degrees of freedom are difficult to be treated in a large size of the system. In addition, it is also important to clarify whether a 1D Mott-Hubbard insulator shows the same non-

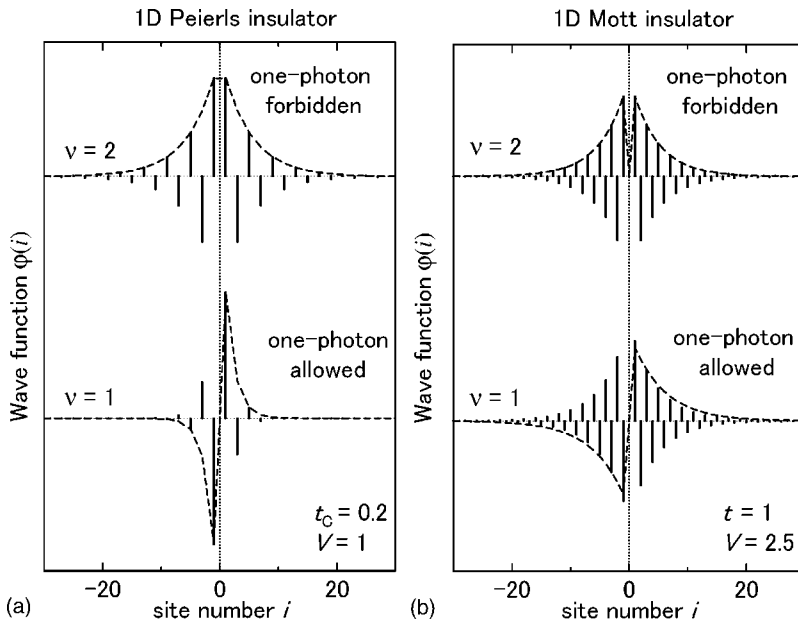


FIG. 14. Electron distributions relative to a hole at $i=0$ for the lowest excited state with odd parity ($\nu=1$) and the second lowest excited state with even parity ($\nu=2$) in a 1D Peierls insulator (a) and a 1D Mott insulator (b). The parameters used for the calculations are $t_C=0.2$, and $V=1$ for a 1D Peierls insulator, and $t=1$, and $V=2.5$ for a 1D Mott insulator.

linear optical properties as the 1D CT insulators or not. Mazumdar *et al.* have calculated the photoexcited states of CT insulators using two-band model and indicated that the lowest odd and even states would degenerate.^{21,23} Further experimental studies about the nonlinear optical properties of 1D Mott–Hubbard insulators, such as organic CT compounds will give important information on this problem.

B. Crossover from excitonic bound states to electron-hole continuum states in the CuO–chain compounds

In this section, we discuss the nature of the photoexcited states in the CuO–chain compounds. As we have reported in Sec. V, the photoexcited states of the CuO chains are somewhat different from those of the NiX chains. From the results of the photoconductivity excitation spectra and the luminescence efficiency, it was argued that the excitonic effect is finite but weak in Sr_2CuO_3 and negligible in Ca_2CuO_3 . In the CuO–chain compounds, such a weak excitonic effect is considered to be the reason why the three-level model cannot fully reproduce the experimental $\chi^{(3)}$ spectra evaluated by the ER spectroscopy. Comparing the $\chi^{(3)}$ spectra of the two CuO–chain compounds, we can discern an important difference in their spectral shapes; the energy of the minimum E_{dip} (denoted by the arrows in Fig. 8 and represented as ω_{dip} in Ref. 17) in $\chi^{(3)}$ which characterizes the energy position of the oscillating structure, is almost equal to E_{CT} in Sr_2CuO_3 , but smaller than E_{CT} in Ca_2CuO_3 . Such a low-energy shift of E_{dip} is associated with the fact that the energy position of the even excited state evaluated by the three-level model is considerably lower than E_{CT} . The difference between the two 1D cuprates is also observed in the $\chi^{(3)}(-3\omega; \omega, \omega, \omega)$ spectra obtained from the THG spectroscopy.¹⁷

To clarify the observed dependence of the $\chi^{(3)}$ spectral shape on the magnitudes of the excitonic effect, Tohyama *et al.* have calculated the linear and nonlinear optical spectra of the 1D cuprates using the holon-doublon model as a function of V/t .¹⁷ According to the calculated results, for $V/t > 2$ the

oscillator strength of the linear absorption concentrates on a bound state of holon and doublon, showing a sharp excitonic peak in ϵ_2 spectra. When $V/t < 2$, the weight of the oscillator strength is distributed over a wide energy region and the peak of ϵ_2 spectrum (E_{CT}) shifts to the higher energy than the absorption edge. Such a feature for large U has been also reported from the other theoretical studies.^{77,86} Tohyama *et al.* have also shown that E_{dip} in $\text{Im}\chi^{(3)}(-\omega; 0, 0, \omega)$ spectrum is almost equal to E_{CT} for $V/t > 2$, but is smaller than E_{CT} for $V/t < 2$. The low-energy shift of E_{dip} for $V/t < 2$ is attributable to the fact that the photoexcited states are composed of many pairs of the odd and even excited states and the weight center for the transition dipole moment between odd- and even-parity states stays around the band edge.

As mentioned in the previous subsection, the values of the parameters in Sr_2CuO_3 have been evaluated to be $t = 0.55$ eV, $V = 1.3$ eV, and $U = 4.2$ eV.⁷⁵ Accordingly, $V/t = 2.4$. In Ca_2CuO_3 , there have been no reliable evaluations for the value of V/t . As mentioned in Sec. III, the Cu–O bond length along the chain is smaller in Ca_2CuO_3 than in Sr_2CuO_3 , that leads to the larger V and t for Ca_2CuO_3 . As shown in previous papers,¹⁷ t is expected to be more sensitive to the bond length than V .⁸⁷ Therefore, V/t is smaller in Ca_2CuO_3 than in Sr_2CuO_3 . Judging from the fact that the excitonic effect is negligible in Ca_2CuO_3 , it is considered that $V/t < 2$ for Ca_2CuO_3 . By taking into account the difference of V/t between the two CuO–chain compounds, we can see that the theoretical results explain the feature of the experimental spectra; E_{dip} is almost equal to E_{CT} in Sr_2CuO_3 , but smaller than E_{CT} in Ca_2CuO_3 . In Ca_2CuO_3 , the low-energy shift of the even excited state deduced from the three-level model analysis on the $\text{Im}\chi^{(3)}(-\omega; 0, 0, \omega)$ spectrum is an artifact coming from the application of the three-level model to the continuous photoexcited states. The distribution of $\langle 0|x|1 \rangle$ as a function of the energy of the odd excited state $|1 \rangle$ is different from that of $\langle 1|x|2 \rangle$. It is, therefore, natural to consider that the odd and even excited states would be also nearly degenerate even in Ca_2CuO_3 .

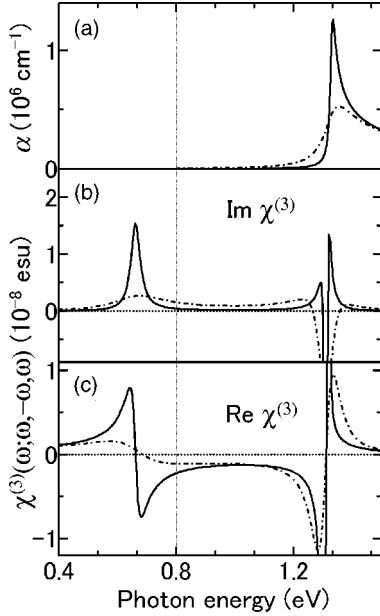


FIG. 15. The calculated absorption $\alpha(\omega)$ (a), $\text{Im}\chi^{(3)}(-\omega; \omega, -\omega, \omega)$ (b) and $\text{Re}\chi^{(3)}(-\omega; \omega, -\omega, \omega)$ (c) spectra for 77 K (the solid lines) and room temperature (the dotted-dashed lines). As for the parameter values of the damping factors at RT, the FWHM of ε_2 at 298 K is used as γ_1 , and γ_2 is determined by assuming the relation $\gamma_2 \sim 5.2\gamma_1$, which is obtained for 77 K.

C. Strategy of exploration for good nonlinear optical materials

According to the results we have obtained in Sec. VI A, 1D Mott insulators are considered to be advantageous for nonlinear optical materials when compared to 1D band or Peierls insulators. For the applications of third-order nonlinear optical materials as optical switching devices, it is most important to realize large $\chi^{(3)}(-\omega; \omega, -\omega, \omega)$ defined as $P(\omega) = 3/4\chi^{(3)}(-\omega; \omega, -\omega, \omega)E(\omega)E(-\omega)E(\omega)$ in a transparent region (or equivalently an off-resonant region). Here, we focus on $\text{Re}\chi^{(3)}(-\omega; \omega, -\omega, \omega)$ at 0.8 eV (1.55 μm) which corresponds to a typical wavelength for optical communication.

As for π -conjugated polymers, $|\text{Re}\chi^{(3)}(-\omega; \omega, -\omega, \omega)|$ around the absorption edge (~ 2 eV) was directly measured using degenerate four wave mixing.⁸⁸ According to the study, $|\text{Re}\chi^{(3)}(-\omega; \omega, -\omega, \omega)|$ for the off-resonant energy of 0.8 eV is much smaller than 10^{-10} esu. Such a measurement of $\chi^{(3)}(-\omega; \omega, -\omega, \omega)$ has not been performed on the 1D Mott insulators presented here. The values of $|\text{Re}\chi^{(3)}(-\omega; \omega, -\omega, \omega)|$, however, can be readily calculated by using the parameters ($E_1 = \hbar\omega_1$, $E_2 = \hbar\omega_2$, $\gamma_{1,2}$, and $\langle 0, 2|x|1 \rangle$) obtained from the fitting procedures on the ε_2 and $\chi^{(3)}(-\omega; 0, 0, \omega)$ spectra. For Ni-Br-Br, the calculated $\text{Im}\chi^{(3)}(-\omega; \omega, -\omega, \omega)$ and $\text{Re}\chi^{(3)}(-\omega; \omega, -\omega, \omega)$ spectra at 77 K and RT are presented in Figs. 15(b) and 15(c), respectively. To evaluate the spectra at RT, the half width at half maximum of ε_2 at 298 K is used as γ_1 . As for γ_2 , there is no experimental datum, so that we assume the relation $\gamma_2 = 5.2\gamma_1$, which was obtained for the case at 77 K. The evaluated values of $|\text{Re}\chi^{(3)}(-\omega; \omega, -\omega, \omega)|$ at 1.55 μm (0.8 eV)

for the three NiX-chain compounds, Sr_2CuO_3 and Ca_2CuO_3 are listed in Table III. They are larger than 10^{-10} esu except for Ni-Cl- NO_3 and Ca_2CuO_3 . Similar calculations have given the $|\text{Re}\chi^{(3)}(-\omega; \omega, -\omega, \omega)|$ values at 0.8 eV less than 10^{-12} esu for PDHS and less than 10^{-10} esu for the PtX-chain compounds. It should be noted that $|\text{Re}\chi^{(3)}(-\omega; \omega, -\omega, \omega)|$ in Ni-Br-Br exceeds 10^{-9} esu, which is, the largest off-resonant value among the 1D semiconductors. Judging from these facts, it can be concluded that the 1D Mott insulators have significantly large third-order optical nonlinearity overwhelming the conventional nonlinear optical materials even in the off-resonant condition.

Finally, we briefly discuss the strategy to explore good nonlinear optical materials in this type of 1D Mott insulators. As seen in Fig. 15, $|\text{Im}\chi^{(3)}(-\omega; \omega, -\omega, \omega)|$ has the maximum at around the half of ω_2 , which is attributed to the two-photon absorption (TPA) resonance to the even excited state. The TPA is accompanied by the dispersion of $|\text{Re}\chi^{(3)}(-\omega; \omega, -\omega, \omega)|$ at the same energy region. $|\text{Re}\chi^{(3)}(-\omega; \omega, -\omega, \omega)|$ has finite values over the wide energy region for $\omega < \omega_1$. In the range for $\omega_2/2 \leq \omega$, $|\text{Re}\chi^{(3)}(-\omega; \omega, -\omega, \omega)|$ increases when the spectral width decreases. Therefore, necessary conditions to realize large $|\text{Re}\chi^{(3)}(-\omega; \omega, -\omega, \omega)|$ at 0.8 eV are considered to be a sharp spectral width as well as large dipole moments $\langle 0|x|1 \rangle$ and $\langle 1|x|2 \rangle$. To utilize $\text{Re}\chi^{(3)}(-\omega; \omega, -\omega, \omega)$ for applications, there should be no linear and nonlinear absorptions, so that the optical gap energy E_{CT} is necessary to be larger than 0.8 eV and smaller than 1.6 eV. In the NiBr-chain compound, these necessary conditions are satisfied and the largest $|\text{Re}\chi^{(3)}(-\omega; \omega, -\omega, \omega)|$ will be observed.

To realize a sharp spectral shape, a finite excitonic effect or a finite excitonic binding energy is necessary, which concentrates the oscillator strength on the lowest odd state. The comparison of the spectral widths between the NiBr and NiCl chain has shown that the spectrum becomes very sharp even if the excitonic binding energy is very small as in the case of the NiBr-chain. The spectrum is necessarily broadened by the e - l interaction, which should be suppressed. In the NiX-chain compounds, the large transfer energy t suppresses the effects of the site-diagonal-type e - l interaction, which leads to a sharp spectral width. The CuO-chain compounds will be disadvantageous, since the excitonic effect is relatively small and the e - l interaction is fairly large.

The transition dipole moments increase with increase of the transfer energy t and decrease of the optical gap. The extremely large V will not be good, since it diminishes the dipole moment between the odd and even excited state. Taking account of the above discussions about the spectral shape, V should be slightly larger than $2t$. From these considerations, we propose that the key factors to obtain a good nonlinear optical material in the 1D Mott insulators are a large transfer energy along the chain sufficient to enhance the transition dipole moments and to suppress the e - l interaction, an appropriate magnitude of optical gap and a small but finite excitonic effect sufficient to stabilize an excitonic bound state.

VII. SUMMARY

We studied the linear and nonlinear optical responses in the 1D Mott insulators of the halogen-bridged Ni compounds

(the NiX–chain compounds) and the CuO–chain compounds.

From the excitation profiles of photoconductivity and the photoluminescence efficiency measurements, we showed that the CT excited states in the NiX chains form excitonic bound states. As compared with the NiX–chain compounds, the excitonic effect is small for Sr₂CuO₃ and negligible for Ca₂CuO₃. The relatively large excitonic effect in the NiX chains is attributable to the strong 1D confinement of the electronic state. From the temperature dependence of the ϵ_2 spectra, we have revealed that the widths Γ_{CT} of the ϵ_2 spectra of the 1D Mott insulators are dominated mainly by the e – l interaction. The extremely small Γ_{CT} in the NiBr–chain compound can be explained by the effective suppression of the e – l interaction, which originates in the large electron itinerancy along the chain.

The $\chi^{(3)}(-\omega;0,0,\omega)$ spectra of the 1D Mott insulators were obtained by the ER spectroscopy. The maximum values of $|\text{Im}\chi^{(3)}(-\omega;0,0,\omega)|$ in the 1D Mott insulators ($\sim 10^{-5}$ – 10^{-8} esu) were considerably larger than those of other 1D semiconductors such as 1D band insulators of polysilane, and 1D Peierls insulators of π -conjugated polymers and the halogen-bridged Pt compounds ($\sim 10^{-8}$ – 10^{-10} esu). To elucidate the enhancement of $|\text{Im}\chi^{(3)}(-\omega;0,0,\omega)|$ in the 1D Mott insulators, we have compared the nature of the photoexcited states of the 1D Mott insulators with those of the 1D band and Peierls insulators. In the 1D Mott insulators, the odd and even CT excited states are nearly degenerate, which induces the large transition dipole moment between these two states and then leads to the enhancement of $\chi^{(3)}$. Such a feature in the 1D Mott insulators is independent of the magnitude of the excitonic effect, although the excitonic effect sharpens the $\chi^{(3)}$ spectrum and then enhances the maximum value of $|\chi^{(3)}|$. In the 1D band and Peierls insulators, on the other hand, both the exciton binding energy and the splitting between the lowest excited state with odd parity and the second-lowest one with even parity are fairly large. It leads to the diminution of the transition dipole moment between these two excited states and results in small $\chi^{(3)}$. These differences of the photoexcited states between the 1D Mott insulators and others have been explained in terms of the 1D extended Peierls–Hubbard model. We have also proposed the strategy to explore good nonlinear optical materials on the basis of the results of the linear and nonlinear optical responses in the 1D Mott insulators.

ACKNOWLEDGMENTS

The authors thank Professor T. Tohyama and Professor S. Maekawa (MRS, Tohoku University), and Dr. K. Iwano (KEK) for many enlightening discussions. We also thank Dr. T. Manabe for the supports of the sample preparations of the Ni compounds at the early stage of this work. This work was supported in part by a Grant-in-Aid from the Ministry of Education, Science, Sports and Culture of Japan.

APPENDIX: TRANSFORMATION OF THE PERTURBED HAMILTONIAN FOR 1D PEIERLS INSULATORS AND 1D MOTT INSULATORS INTO SIMPLE TWO- AND THREE-IMPURITY MODELS

Here, we will show how to transform the perturbed Hamiltonian for the 1D Peierls insulator and the 1D Mott

insulator into a simple two- and three-impurity model, respectively. First, we focus on the 1D Peierls insulator. In Sec. VI A, we have introduced the perturbed Hamiltonian for the 1D Peierls insulator as Eq. (5). A photoexcited state in this system is expressed as the sum of an electron-hole pair, whose electron and hole are i sites apart from each other. Its wave function is given as follows:

$$|\psi_{PI}\rangle = \frac{1}{\sqrt{2}} \sum_{i,l,\sigma} \phi(i) a_{2l+i,\sigma}^+ b_{2l,-\sigma}^+ |0\rangle, \quad (\text{A1})$$

where $\phi(i)$ stands for the wave function of the relative coordinate and $|0\rangle$ is the ground state. Since an electron and a hole can transfer only to odd number and even number sites, respectively, it is restricted that i must be an odd number. We put (5) and (A1) in $H_{PI}|\Psi_{PI}\rangle$, we obtain the first term and the second term as follows:

$$\begin{aligned} & \frac{1}{\sqrt{2}} t_C \sum_{i,l',\sigma,\sigma'} \phi(i) (a_{2l+1,\sigma}^+ a_{2l-1,\sigma} \\ & + a_{2l-1,\sigma}^+ a_{2l+1,\sigma}^+) a_{2l'+i,\sigma'}^+ b_{2l',-\sigma'}^+ |0\rangle \\ & = \frac{1}{\sqrt{2}} t_C \sum_{l,i,\sigma} \phi(i) (a_{2l+i+2,\sigma}^+ b_{2l,-\sigma}^+ + a_{2l+i-2,\sigma}^+ b_{2l,-\sigma}^+) |0\rangle \\ & = \frac{1}{\sqrt{2}} t_C \sum_{l,i,\sigma} [\phi(i-2) + \phi(i+2)] a_{2l+i,\sigma}^+ b_{2l,-\sigma}^+ |0\rangle \end{aligned} \quad (\text{A2})$$

$$\begin{aligned} & \frac{1}{\sqrt{2}} t_C \sum_{i,l',l,\sigma,\sigma'} \phi(i) (b_{2l+2,\sigma}^+ b_{2l,\sigma}^+ + b_{2l,\sigma}^+ b_{2l+2,\sigma}^+) a_{2l'+i,\sigma'}^+ b_{2l',-\sigma'}^+ |0\rangle \\ & = \frac{1}{\sqrt{2}} t_C \sum_{l,i,\sigma} (\phi(i-2) + \phi(i+2)) a_{2l+i,\sigma}^+ b_{2l,-\sigma}^+ |0\rangle. \end{aligned} \quad (\text{A3})$$

Following the same scheme, the third term is given as follows.

$$\begin{aligned} & \frac{1}{\sqrt{2}} V \sum_{i,l',l,\sigma,\sigma'} \phi(i) (a_{2l+1,\sigma}^+ a_{2l+1,\sigma}^+ b_{2l,-\sigma}^+ b_{2l,-\sigma}^+ \\ & + b_{2l,-\sigma}^+ b_{2l,-\sigma}^+ a_{2l-1,\sigma}^+ a_{2l-1,\sigma}^+) a_{2l'+i,\sigma'}^+ b_{2l',-\sigma'}^+ |0\rangle \\ & = \frac{1}{\sqrt{2}} V \sum_{l,i,\sigma} (\delta_{1,i} + \delta_{-1,i}) a_{2l+i,\sigma}^+ b_{2l,-\sigma}^+ |0\rangle. \end{aligned} \quad (\text{A4})$$

As a result, $H_{PI}|\psi_{PI}\rangle$ can be transformed to the following formulas:

$$\begin{aligned} H_{PI}|\psi_{PI}\rangle & = \sum_{i,l,\sigma} \{2t_C [\phi(i-2) + \phi(i+2)] \\ & - V(\delta_{1,i} + \delta_{-1,i})\} \frac{1}{\sqrt{2}} a_{2l+i,\sigma}^+ b_{2l,-\sigma}^+ |0\rangle. \end{aligned} \quad (\text{A5})$$

The effective Hamiltonian for electrons can be expressed as,

$$\tilde{H}_{PI} = 2t_C \sum_i (|i-2\rangle\langle i| + |i+2\rangle\langle i|) - V(|1\rangle\langle 1| + |-1\rangle\langle -1|), \quad (\text{A6})$$

where $|i\rangle$ stands for the state that an electron exists at i th site. It is equivalent to that of a system having two impurities embedded in a periodic tight-binding model as shown in Fig. 12(a-2).

The Hamiltonian for the 1D Mott insulator is shown as Eq. (6). Creation and annihilation operators, a_i^+ , a_i , and b_i^+ , b_i in Eq. (6) indicates those of holon and doublon. In Eq. (6), we set $V' \rightarrow \infty$. The photoexcited state will be represented as

$$|\psi_{MI}\rangle = \sum_{i,l} \phi(i) a_{i+l}^+ b_l^+ |0\rangle. \quad (\text{A7})$$

From Eqs. (6) and (A7), we obtain an effective Hamiltonian presented below:

$$\begin{aligned} \tilde{H}_{MI} = 2t_M \sum_i (|i-1\rangle\langle i| + |i+1\rangle\langle i|) - V(|1\rangle\langle 1| + |-1\rangle\langle -1|) \\ + V'|0\rangle\langle 0|. \end{aligned} \quad (\text{A8})$$

This Hamiltonian is equal to the simple Hamiltonian of the three-impurity model, where two impurities with the energy of $-V$ locate at the sites $i=\pm 1$ and another impurity with the energy of V' ($\rightarrow \infty$) is located at the site $i=0$, as shown in Fig. 12(b-2). The discrete energy levels and the wave functions of the trapped states are given as solutions of the exactly solvable Green's function.⁸¹

*Present address: Institute for Materials Research, Tohoku University, Sendai 980-8577, Japan.

†Author to whom correspondence should be addressed. Electronic address: okamoto@k.u-tokyo.ac.jp

¹J. R. G. Thorne, Y. Ohsako, J. M. Zeigler, and R. M. Hochstrasser, *Chem. Phys. Lett.* **162**, 455 (1989).

²Z. G. Soos and R. G. Kepler, *Phys. Rev. B* **43**, 11908 (1991).

³R. G. Kepler and Z. G. Soos, *Phys. Rev. B* **43**, 12530 (1991).

⁴T. Hasegawa, Y. Iwasa, T. Koda, H. Kishida, Y. Tokura, S. Wada, H. Tashiro, H. Tachibana, and M. Matsumoto, *Phys. Rev. B* **54**, 11365 (1996).

⁵H. Tachibana, M. Matsumoto, Y. Tokura, Y. Moritomo, A. Yamaguchi, S. Koshihara, R. D. Miller, and S. Abe, *Phys. Rev. B* **47**, 4363 (1993).

⁶D. S. Chemla and J. Zyss, *Nonlinear Optical Properties of Organic Molecules and Crystals* (Academic, New York, 1987), Vols. 1 and 2, and references therein.

⁷W.-S. Fann, S. Benson, J. M. J. Madey, S. Etemad, G. L. Baker, and F. Kajzar, *Phys. Rev. Lett.* **62**, 1492 (1989).

⁸C. Sautret, J.-P. Hermann, R. Frey, F. Pradere, J. Ducuing, R. H. Baughman, and R. R. Chance, *Phys. Rev. Lett.* **36**, 956 (1976).

⁹D. Guo, S. Mazumdar, S. N. Dixit, F. Kajzar, F. Jarka, Y. Kawabe, and N. Peyghambarian, *Phys. Rev. B* **48**, 1433 (1993).

¹⁰S. Abe, M. Schreiber, W. P. Su, and J. Yu, *Phys. Rev. B* **45**, 9432 (1992).

¹¹P. C. M. McWilliams, G. W. Hayden, and Z. G. Soos, *Phys. Rev. B* **43**, 9777 (1991).

¹²Y. Tokura, Y. Oowaki, T. Koda, and R. H. Baughmann, *Chem. Phys.* **88**, 437 (1984).

¹³Y. Wada and M. Yamashita, *Phys. Rev. B* **42**, 7398 (1990).

¹⁴Y. Iwasa, E. Funatsu, T. Hasegawa, T. Koda, and M. Yamashita, *Appl. Phys. Lett.* **59**, 2219 (1991).

¹⁵G. S. Kanner, G. F. Strouse, B. I. Swanson, M. Sinclair, J. P. Jiang, and N. Peyghambarian, *Phys. Rev. B* **56**, 2501 (1997).

¹⁶H. Kishida, H. Matsuzaki, H. Okamoto, T. Manabe, M. Yamashita, Y. Taguchi, and Y. Tokura, *Nature (London)* **405**, 929 (2000).

¹⁷H. Kishida, M. Ono, K. Miura, H. Okamoto, M. Izumi, T. Manako, M. Kawasaki, Y. Taguchi, Y. Tokura, T. Tohyama, K.

Tsutsui, and S. Maekawa, *Phys. Rev. Lett.* **87**, 177401 (2001).

¹⁸S. D. Phillips, R. Worland, G. Yu, T. Hagler, R. Freedman, Y. Cao, V. Yoon, J. Chiang, W. C. Walker, and A. J. Heeger, *Phys. Rev. B* **40**, 9751 (1989).

¹⁹Y. Tokura, T. Koda, A. Itsubo, M. Miyabayashi, K. Okuhara, and A. Ueda, *J. Chem. Phys.* **85**, 99 (1986).

²⁰O. M. Gelsen, D. D. C. Bradley, H. Murata, N. Nakada, T. Tsutsui, and S. Saito, *J. Appl. Phys.* **71**, 1064 (1992).

²¹T. Ogasawara, M. Ashida, N. Motoyama, H. Eisaki, S. Uchida, Y. Tokura, H. Ghosh, A. Shukla, S. Mazumdar, and M. Kuwata-Gonokami, *Phys. Rev. Lett.* **85**, 2204 (2000).

²²Y. Mizuno, K. Tsutsui, T. Tohyama, and S. Maekawa, *Phys. Rev. B* **62**, R4769 (2000).

²³M. Ashida, T. Ogasawara, Y. Tokura, S. Uchida, R. T. Clay, S. Mazumdar, and M. Kuwata-Gonokami, *Europhys. Lett.* **58**, 455 (2002).

²⁴K. Toriumi, Y. Wada, T. Mitani, S. Bandow, M. Yamashita, and Y. Fujii, *J. Am. Chem. Soc.* **111**, 2341 (1989).

²⁵K. Toriumi, H. Okamoto, T. Mitani, S. Bandow, M. Yamashita, Y. Wada, Y. Fujii, R. J. Clark, D. J. Michael, A. J. Edward, D. Watkin, M. Kurmoo, and P. Day, *Mol. Cryst. Liq. Cryst.* **181**, 333 (1990).

²⁶M. Yamashita, K. Inoue, T. Tsuruta, A. Ichikawa, H. Okamoto, N. Kimura, H. Ohki, R. Ikeda, H. Kitagawa, S. Bandow, K. Toriumi, T. Mitani, T. Ohnishi, and H. Miyake, *Mol. Cryst. Liq. Cryst. Sci. Technol., Sect. A* **256**, 179 (1994).

²⁷H. Okamoto, H. Kishida, M. Ono, H. Matsuzaki, M. Yamashita, and T. Manabe, *J. Lumin.* **87-89**, 204 (2000).

²⁸H. Okamoto, Y. Shimada, Y. Oka, A. Chainani, T. Takahashi, H. Kitagawa, T. Mitani, K. Toriumi, K. Inoue, T. Manabe, and M. Yamashita, *Phys. Rev. B* **54**, 8438 (1996).

²⁹M. Yamashita, T. Manabe, T. Kawashima, H. Okamoto, and H. Kitagawa, *Coord. Chem. Rev.* **190-192**, 309 (1999).

³⁰H. Okamoto, K. Toriumi, T. Mitani, and M. Yamashita, *Phys. Rev. B* **42**, 10381 (1990).

³¹K. Okaniwa, H. Okamoto, T. Mitani, K. Toriumi, and M. Yamashita, *J. Phys. Soc. Jpn.* **60**, 997 (1991).

³²H. Okamoto and M. Yamashita, *Bull. Chem. Soc. Jpn.* **71**, 2023 (1998).

- ³³Chr. L. Teske and H. M.-Buschbaum, *Z. Anorg. Allg. Chem.* **379**, 234 (1969).
- ³⁴Chr. L. Teske and H. M.-Buschbaum, *Z. Anorg. Allg. Chem.* **370**, 234 (1970).
- ³⁵K. Marumoto, H. Tanaka, S. Kuroda, T. Manabe, and M. Yamashita, *Phys. Rev. B* **60**, 7699 (1999).
- ³⁶M. Ono and H. Okamoto (unpublished).
- ³⁷N. Motoyama, H. Eisaki, and S. Uchida, *Phys. Rev. Lett.* **76**, 3212 (1996).
- ³⁸J. Zaanen, G. A. Sawatzky, and J. W. Allen, *Phys. Rev. Lett.* **55**, 418 (1985).
- ³⁹F. C. Zhang and T. M. Rice, *Phys. Rev. B* **37**, 3759 (1988).
- ⁴⁰Y. Ohta, T. Tohyama, and S. Maekawa, *Phys. Rev. Lett.* **66**, 1228 (1991).
- ⁴¹R. Loudon, *Am. J. Phys.* **27**, 649 (1959).
- ⁴²R. J. Elliot and R. Loudon, *J. Phys. Chem. Solids* **15**, 196 (1960).
- ⁴³T. Ogawa and T. Takagahara, *Phys. Rev. B* **44**, 8138 (1991).
- ⁴⁴F. Kajzar, J. Messier, and C. Rosilio, *J. Appl. Phys.* **60**, 3040 (1986); J. R. G. Thorne, Y. Ohsako, J. M. Zeigler, and R. M. Hochstrasser, *Chem. Phys. Lett.* **162**, 455 (1989).
- ⁴⁵Z. G. Soos, S. Ramasesha, and D. S. Galvao, *Phys. Rev. Lett.* **71**, 1609 (1993).
- ⁴⁶S. Abe, J. Yu, and W. P. Su, *Phys. Rev. B* **45**, 8264 (1992).
- ⁴⁷M. Liess, S. Jeglinski, Z. V. Vardeny, M. Ozaki, K. Yoshino, Y. Ding, and T. Barton, *Phys. Rev. B* **56**, 15712 (1997).
- ⁴⁸K. Lochner, H. Bassler, B. Tieke, and G. Weigner, *Phys. Status Solidi B* **88**, 653 (1978).
- ⁴⁹Y. Nakai and K. Teegarden, *J. Phys. Chem. Solids* **22**, 327 (1961).
- ⁵⁰G. Kuwabara and K. Aoyagi, *J. Phys. Chem. Solids* **22**, 333 (1961).
- ⁵¹L. Sebastian and G. Weiser, *Phys. Rev. Lett.* **46**, 1156 (1981).
- ⁵²S. Abe, *J. Phys. Soc. Jpn.* **58**, 62 (1989).
- ⁵³R. S. Knox, *Theory of Excitons* (Academic, New York, 1963).
- ⁵⁴B. M. Craven, *Acta Crystallogr.* **14**, 475 (1961).
- ⁵⁵S. Tomimoto, S. Saito, T. Suemoto, J. Takeda, and S. Kurita, *Phys. Rev. B* **66**, 155112 (2002).
- ⁵⁶The frequency of the LO-phonon mode was calculated using the parameters values given, see, for example Y. S. Lee, T. W. Noh, H. S. Choi, E. J. Choi, H. Eisaki, and S. Uchida, *Phys. Rev. B* **62**, 5285 (2000).
- ⁵⁷O. V. Misocho, S. Tajima, C. Urano, H. Eisaki, and S. Uchida, *Phys. Rev. B* **53**, R14733 (1996).
- ⁵⁸R. J. McQueeney, Y. Petrov, T. Egami, M. Yethiraj, G. Shirane, and Y. Endoh, *Phys. Rev. Lett.* **53**, 628 (1999).
- ⁵⁹M. Yoshida, S. Tajima, N. Koshizuka, S. Tanaka, S. Uchida, and S. Ishibashi, *Phys. Rev. B* **44**, 11997 (1991).
- ⁶⁰K. Iwano, M. Ono, and H. Okamoto, *Phys. Rev. B* **66**, 235103 (2002).
- ⁶¹W. Franz, *Z. Naturforsch. A* **13a**, 484 (1958).
- ⁶²L. V. Keldysh, *Zh. Eksp. Teor. Fiz.* **7**, 1138 (1958).
- ⁶³T. Hasegawa, K. Ishikawa, T. Koda, K. Takeda, H. Kobayashi, and K. Kubodera, *Synth. Met.* **43**, 3151 (1991).
- ⁶⁴L. Sebastian and G. Weiser, *Chem. Phys.* **62**, 447 (1981).
- ⁶⁵S. N. Dixit, D. Guo, and S. Mazumdar, *Phys. Rev. B* **43**, 6781 (1991).
- ⁶⁶P. N. Butcher and D. Cotter, *The Elements of Nonlinear Optics* (Cambridge University Press, Cambridge, 1990).
- ⁶⁷In the previous paper (Ref. 17), we performed the fitting by setting γ_1 as a fitting parameter as well as γ_2 and $\langle 1|x|2\rangle$. Therefore, the results of the fitting presented here are slightly different from those reported in Ref. 17.
- ⁶⁸C. J. Baker, O. M. Gelsen, and D. D. C. Bradley, *Chem. Phys. Lett.* **201**, 127 (1993).
- ⁶⁹The electroabsorption of PDHS has already been reported by H. Tachibana *et al.* (Ref. 5). However, the measurement was done with the electric field applied normal to the PDHS film and in that case, the absolute value of $\chi^{(3)}$ cannot be obtained. Therefore, we examined the absolute value of $\chi^{(3)}$ of PDHS by EA measurement applying the electric field parallel to the film.
- ⁷⁰These parameters are extracted from Ref. 13.
- ⁷¹R. D. Miller and J. Michl, *Chem. Rev. (Washington, D.C.)* **89**, 1359 (1989).
- ⁷²H. Eskes and G. A. Sawatzky, *Phys. Rev. Lett.* **61**, 1415 (1988).
- ⁷³S. I. Fujimori, A. Ino, T. Okane, A. Fujimori, K. Okada, T. Manabe, M. Yamashita, H. Kishida, and H. Okamoto, *Phys. Rev. Lett.* **88**, 247601 (2002).
- ⁷⁴T. Tohyama and S. Maekawa, *J. Lumin.* **94**, 659 (2001).
- ⁷⁵R. Neudert, M. Knupfer, M. S. Golden, J. Fink, W. Stephan, K. Penc, N. Motoyama, H. Eisaki, and S. Uchida, *Phys. Rev. Lett.* **81**, 657 (1998).
- ⁷⁶Z. Shuai, S. K. Pati, W. P. Su, J. L. Bredas, and S. Ramasesha, *Phys. Rev. B* **55**, 15368 (1997).
- ⁷⁷F. B. Gallagher and S. Mazumdar, *Phys. Rev. B* **56**, 15025 (1997).
- ⁷⁸M. Haruki, M. Tanaka, and S. Kurita, *Synth. Met.* **19**, 901 (1987).
- ⁷⁹C. Kim, A. Y. Matsuura, Z.-X. Shen, N. Motoyama, H. Eisaki, S. Uchida, T. Tohyama, and S. Maekawa, *Phys. Rev. Lett.* **77**, 4054 (1996).
- ⁸⁰W. Stephan and K. Penc, *Phys. Rev. B* **54**, R17269 (1996).
- ⁸¹E. N. Economou, *Green's Functions in Quantum Physics* (Springer-Verlag, Berlin, 1983).
- ⁸²According to the previous theoretical study on the PtX chain [K. Iwano and K. Nasu *J. Phys. Soc. Jpn.* **61**, 1380 (1992)], the parameter value of t is almost equal to the half of the optical gap energy E_{CT} ($\sim \delta$). In this case, t_c will be slightly larger than 0.2, but the relation between E_b and V shown in Fig. 13 for the 1D Peierls insulator is essentially unchanged.
- ⁸³B. F. Gebhard, K. Bott, M. Scheidler, P. Thomas, and S. W. Koch, *Philos. Mag. B* **75**, 47 (1997).
- ⁸⁴F. H.L. Essler, F. Gebhard, and E. Jeckelmann, *Phys. Rev. B* **64**, 125119 (2001).
- ⁸⁵The dependence of E_b on the intersite Coulomb interaction V for the states denoted as $\nu=1$ in Fig. 13 is essentially the same as that of the undimerized case in Fig. 4 of Ref. 77, see F. B. Gallagher and S. Mazumdar.
- ⁸⁶E. Jeckelmann, *Phys. Rev. B* **67**, 075106 (2003).
- ⁸⁷W. A. Harrison, *Electronic Structure and the Properties of Solids: The Physics of the Chemical Bond* (W.H. Freeman, San Francisco, 1980).
- ⁸⁸C. Bubeck, A. Kaltbeitzel, A. Grund, and M. LeClerc, *Chem. Phys.* **154**, 343 (1991).